iScience

CellPress
OPEN ACCESS

Article

Age and Sex Influence Mitochondria and Cardiac Health in Offspring Exposed to Maternal Glucolipotoxicity

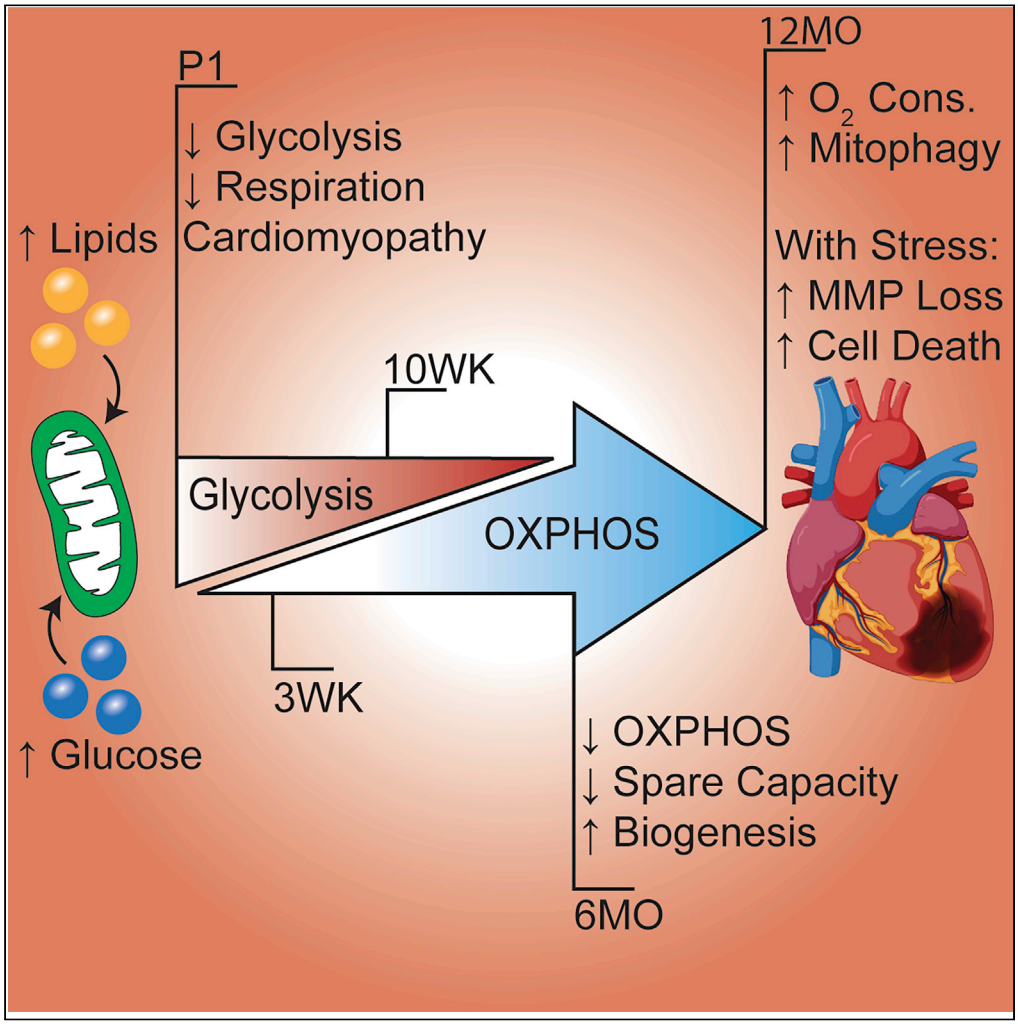

Eli J. Louwagie, Tricia D. Larsen, Angela L. Wachal, ..., Ruthellen H. Anderson, Kennedy S. Mdaki, Michelle L. Baack

eli.louwagie@coyotes.usd.edu (E.J.L.)
michelle.baack@sanfordhealth.org (M.L.B.)

HIGHLIGHTS

Fetal exposures disrupt mitochondria, bioenergetics, & cardiac function at birth

First, bioenergetics & function improve until greater reliance on OXPHOS with age

At 6MO, poor respiration incites biogenesis & mitophagy, and then functional decline

Fetal exposures cause faster mitochondria-mediated cell death in aged adult hearts

Louwagie et al., iScience *23*, 101746
November 20, 2020
https://doi.org/10.1016/j.isci.2020.101746

iScience

CellPress
OPEN ACCESS

Article

Age and Sex Influence Mitochondria and Cardiac Health in Offspring Exposed to Maternal Glucolipotoxicity

Eli J. Louwagie,[1,2,*] Tricia D. Larsen,[2] Angela L. Wachal,[2] Tyler C.T. Gandy,[2] Julie A. Eclov,[2] Todd C. Rideout,[3] Katherine A. Kern,[3] Jacob T. Cain,[2] Ruthellen H. Anderson,[1,2] Kennedy S. Mdaki,[2] and Michelle L. Baack[1,2,4,5,*]

SUMMARY

Infants of diabetic mothers are at risk of cardiomyopathy at birth and myocardial infarction in adulthood, but prevention is hindered because mechanisms remain unknown. We previously showed that maternal glucolipotoxicity increases the risk of cardiomyopathy and mortality in newborn rats through fuel-mediated mitochondrial dysfunction. Here we demonstrate ongoing cardiometabolic consequences by cross-fostering and following echocardiography, cardiomyocyte bioenergetics, mitochondria-mediated turnover, and cell death following metabolic stress in aged adults. Like humans, cardiac function improves by weaning with no apparent differences in early adulthood but declines again in aged diabetes-exposed offspring. This is preceded by impaired oxidative phosphorylation, exaggerated age-related increase in mitochondrial number, and higher oxygen consumption. Prenatally exposed male cardiomyocytes have more mitolysosomes indicating high baseline turnover; when exposed to metabolic stress, mitophagy cannot increase and cardiomyocytes have faster mitochondrial membrane potential loss and mitochondria-mediated cell death. Details highlight age- and sex-specific roles of mitochondria in developmentally programmed adult heart disease.

INTRODUCTION

Babies born to mothers with diabetes or obesity are at greater risk of cardiovascular disease (CVD) (Agarwal et al., 2018; Dong et al., 2013) including cardiomyopathy at birth (Ren et al., 2011; Zablah et al., 2017) and premature death from acute myocardial infarction (AMI) in adulthood (Clausen et al., 2009; Reynolds et al., 2013; Stuart et al., 2013; Yu et al., 2019). This is particularly alarming because over 10% of pregnancies are complicated by gestational diabetes (Sacks et al., 2012) and over 25% by maternal obesity (Gregor et al., 2016), adding to a growing burden of CVD estimated to affect 40% of the US population and cost $818 billion by 2030 (Heidenreich et al., 2011). Developmental consequences are purportedly caused by *in utero* exposure to maternal hyperglycemia and hyperlipidemia (together termed glucolipotoxicity), which incite fetal hyperinsulinemia to program long-term cardiometabolic risks (Barbour, 2019; Cerf, 2018; Freinkel, 1980; Friedman, 2015; Silveira et al., 2007). We previously showed that newborn rats born to diabetic mothers have larger hearts, diastolic and systolic dysfunction, impaired cellular bioenergetics and mitochondrial dysfunction at birth, and maternal high-fat (HF) diet-exacerbated cardiac pathology and perinatal mortality (Baack et al., 2016; Larsen et al., 2019; Louwagie et al., 2018; Mdaki et al., 2016a). Here long-term studies assess risks over a lifetime to highlight age- and sex-specific alterations in cellular bioenergetics, mitophagy, and cell death and resolve underlying mitochondria-mediated mechanisms of adult heart disease, specifically as it relates to cardiac damage following AMI.

Mitochondria play pivotal roles in cardiac development and disease (Gustafsson and Dorn, 2019; Ong et al., 2017). During and after development they directly influence metabolism and cell fate (Mitra, 2013; Perestrelo et al., 2018; Seo et al., 2018). As the primary producers of ATP, mitochondria play an especially important role in the heart, which uses 5–10 times its weight in ATP each day to support contractile function (Lopaschuk and Dhalla, 2014; Murphy et al., 2016). Even the slightest decrease in efficiency can have a profound impact on cardiac function (Ashrafian et al., 2007) causing hypertrophy and systolic and diastolic

[1]University of South Dakota Sanford School of Medicine, Sioux Falls, SD 57105, USA

[2]Environmental Influences on Health and Disease Group, Sanford Research, Sioux Falls, SD 57104, USA

[3]Department of Exercise and Nutrition Sciences, State University of New York, Buffalo, NY 14214, USA

[4]Boekelheide Neonatal Intensive Care Unit, Sanford Children's Hospital, Sioux Falls, SD 57117, USA

[5]Lead Contact

*Correspondence: eli.louwagie@coyotes.usd.edu (E.J.L.), michelle.baack@sanfordhealth.org (M.L.B.)

https://doi.org/10.1016/j.isci.2020.101746

dysfunction (Bugger and Abel, 2014). Mitochondria serve as regulatory hubs to balance fuel supply and energy demand through oxygen-, fuel-, and insulin-mediated pathways that orchestrate tissue-specific metabolic homeostasis through self-replication and respiratory complex assembly (Kodde et al., 2007). Metabolic adaptability is essential to maintain cardiac ATP production during metabolic shifts during rest, exercise, fed, fasting, aerobic, and anaerobic states.

Over the course of development, cardiac metabolism shifts from glycolysis to oxidative phosphorylation (OXPHOS) (Lopaschuk and Jaswal, 2010; Mdaki et al., 2016b). With a relatively low workload and oxygen supply but a continuous source of fuel, the fetal heart relies on glycolytic metabolism. At birth, cardiac metabolism must transition to OXPHOS of stored fuels. This switch is supported by mitochondrial biogenesis, formation of a densely packed mitochondrial reticulum, and tighter respiratory coupling (Dorn et al., 2015; Hollander et al., 2014). Although this developmental shift is necessary, a higher number of dysfunctional mitochondria would consume more oxygen at baseline, have lower reserve capacity, and increase reactive oxygen species (ROS) production, which could incite more cardiac damage during metabolic stress. When mitochondria are damaged, mitochondrial membrane potential (MMP) loss signals degradation via mitophagy (Kubli and Gustafsson, 2012). Physiologic mitophagy is beneficial for culling dysfunctional mitochondria to optimize cellular respiration (Nah et al., 2017), and overload of dysfunctional mitochondria can cause cell death by several pathways including mitochondria-mediated intrinsic apoptosis or mitochondrial permeability transition (MPT)-driven necrosis (Galluzzi et al., 2018) (Figure S6A). The elaborate balance between mitochondrial biogenesis and mitophagy maintains mitochondrial quality control and is tightly controlled by the mediators of mitochondrial dynamism (Pickles et al., 2018). Thus, with aging, mitochondrial dysfunction contributes not only to poor contractile function from impaired bioenergetics but also to greater risk of permanent damage following ischemia-reperfusion injury.

This study builds upon previous work to determine whether fuel-mediated mitochondrial dysfunction found in prenatally exposed offspring at birth disturbs cardiometabolic maturation or mitochondrial quality control during normal development and aging to increase the risk of CVD in adulthood. To assure long-term differences were caused by fetal rather than postnatal exposures, pups were cross-fostered to normal dams in equalized litters for evaluation at predetermined endpoints. Cardiac morphometry and function was followed using echocardiography at newborn (postnatal day 1 [P1]), weaning (3 weeks [WK]), young- [10WK], mid- (6 months [MO]), and aged-adult [12MO] time points. Bioenergetics were measured using extracellular flux analyses of whole and permeabilized primary cardiomyocytes (CM), and temporal relationships were examined to detect developmental aberrations, which is important because change in bioenergetics may be causal or responsive to changes in cardiac function. Adapting reported methods to study MMP (Elmore et al., 2001), mitophagy (Berezhnov et al., 2016), and cell death (Krysko et al., 2008) we developed a reproducible assay to quantify baseline physiologic mitophagy and stress-induced mitochondria-mediated CM death as a cellular "heart attack in a dish." Here, we demonstrate that fetal exposure to maternal glucolipotoxicity alters normal developmental shifts in cardiac metabolism and increases the risk of heart disease in adulthood through mitochondria-mediated mechanisms.

RESULTS

In Utero Exposure to Maternal Glucolipotoxicity Increases Offspring Mortality, Even when Newborns Are Reared by Normal Mothers

We have used a well-characterized rat model to study individual and compounding consequences of late-gestation diabetes, maternal HF diet, and the combination of maternal, placental, and newborn offspring outcomes (Baack et al., 2016; Larsen et al., 2019; Louwagie et al., 2018; Mdaki et al., 2016a; Upadhyaya et al., 2017). To date, we have evaluated 1,265 offspring from 118 litters (29 controls, 29 diabetes-exposed, 32 diet-exposed, and 28 combination-exposed). The model consistently exposes developing offspring to a triad of maternal hyperglycemia, hyperlipidemia, and fetal hyperinsulinemia in the last third of pregnancy. All live-born offspring had cardiac function evaluated by echocardiography on P1. Litters were culled to equal size and cross-fostered to normal dams for follow-up at 3WK, 10WK, 6MO, and 12MO (Figure 1A). The complete course of 72 offspring (n = 15–21/group) from 21 litters (n = 5–6/group) was followed from P1 to 12MO. Maternal and offspring characteristics are shown in Tables S1 and S2. Consistently, dams on HF diet (n = 60) gain more weight than peers on control diet (n = 58). Diabetic dams (n = 57) have hyperglycemia in the last third of pregnancy;

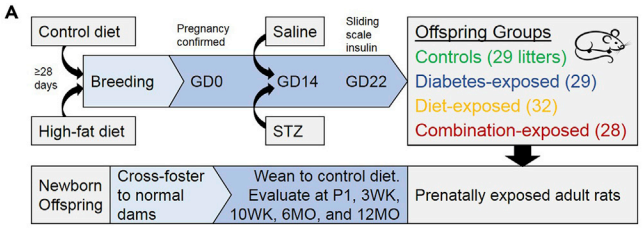

B

Group	N (total)	Perinatal moralities, N (%)	N (aged past P1)	P1 to 12MO mortality, N (%)
Controls	328	32 (9.8)	95	0 (0.0)
Diabetes -exposed	314	39 (12.4)	100	3 (3.0)
HF Diet -exposed	321	***72 (22.4)**	71	3 (4.2)
Combination -exposed	307	***79 (25.7)**	69	7 (10.1)

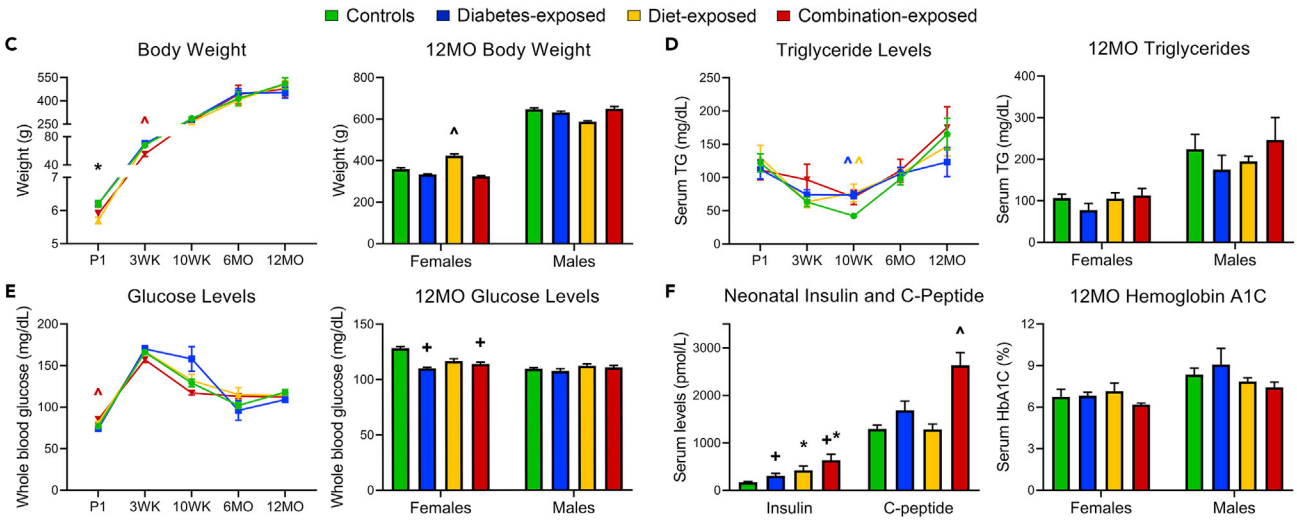

Figure 1. Maternal Glucolipotoxicity Increases Offspring Mortality Despite Little Evidence of Metabolic Syndrome

(A) Sprague Dawley rat model to study offspring cardiometabolic health following fetal exposure to late-gestation diabetes and maternal high-fat (HF) diet.

(B) Perinatal and natural long-term mortality of control and exposed offspring.

(C–E) Offspring weight (C), serum triglyceride levels (D), and whole blood glucose levels (E) over time with 12MO offspring delineated by sex. N_{P1} = 216–250 offspring/group, N_{3WK} = 27–41, N_{10WK} = 21–35, N_{6MO} = 4–9, N_{12MO} = 15–20 (C and E); N_{P1} = 32–57, $N_{3WK,10WK}$ = 14–24, N_{6MO} = 9–10, N_{12MO} = 15–16 (D).

(F) Neonatal insulin, C-peptide, and 12MO hemoglobin A1C levels. N_{P1} = 75–137, N_{12MO} = 8.

Although not marked, body weight (A) and TG levels (D) were significantly higher in males than females. Data represent mean ± SEM. $p \leq 0.05$: $^{+}$diabetes or *diet effect by two-way ANOVA, ^group effect by 1-way ANOVA and Dunnett post-hoc test when interaction by two-way ANOVA was significant.

See also Tables S1 and S2 and Figure S1.

blood glucose levels are maintained at 200–400mg/dL using twice-daily sliding scale insulin. HF diet in combination with streptozocin-induced diabetes increases insulin needs (22 ± 3 total units from GD15-21 versus 19 ± 3 units with diabetes alone), but with sliding scale treatment, diabetic and combination dams have no significant diet-related difference in blood glucose. Ketone, serum triglyceride (TG), and non-esterified fatty acid (NEFA) levels are higher in diabetic and HF diet-fed dams; TG and NEFA are approximately 2-fold higher in diabetic dams, 2- to 3-fold higher in HF-fed dams, and 4- to 5-fold higher in combination. Total and high-density lipoprotein (HDL) cholesterol are not different, but dams on HF diet have higher non-HDL cholesterol. Although litter size does not vary by group, newborn offspring born to HF-fed dams have a 13% higher perinatal mortality rate regardless of diabetic status (Figure 1B). Perinatal mortality is attributed to a combination of stillbirths (Louwagie et al., 2018), pulmonary hypertension (Baack et al., 2016), and cardiomyopathy (Mdaki et al., 2016a). After P1, surviving diet-exposed offspring trend toward higher natural mortality over time ($p = 0.086$) with most deaths occurring between P1 and 3WK and combination-exposed offspring at greatest risk (10%).

Maternal Glucolipotoxicity Increases Cardiac Mass and Impairs Function in Newborn and Aged Offspring with an Intermediate Normalization Period

Full morphometric and functional measurements are detailed in Table S3, and age-related differences are summarized in Table S4. As expected, normal rats have significant growth over time with a ~60- and 100-fold increase in body weight for females and males, respectively. Heart size increases correspondingly with a ~35- and 40-fold increase in heart weight and ~30- and 50-fold increase in left ventricular mass from

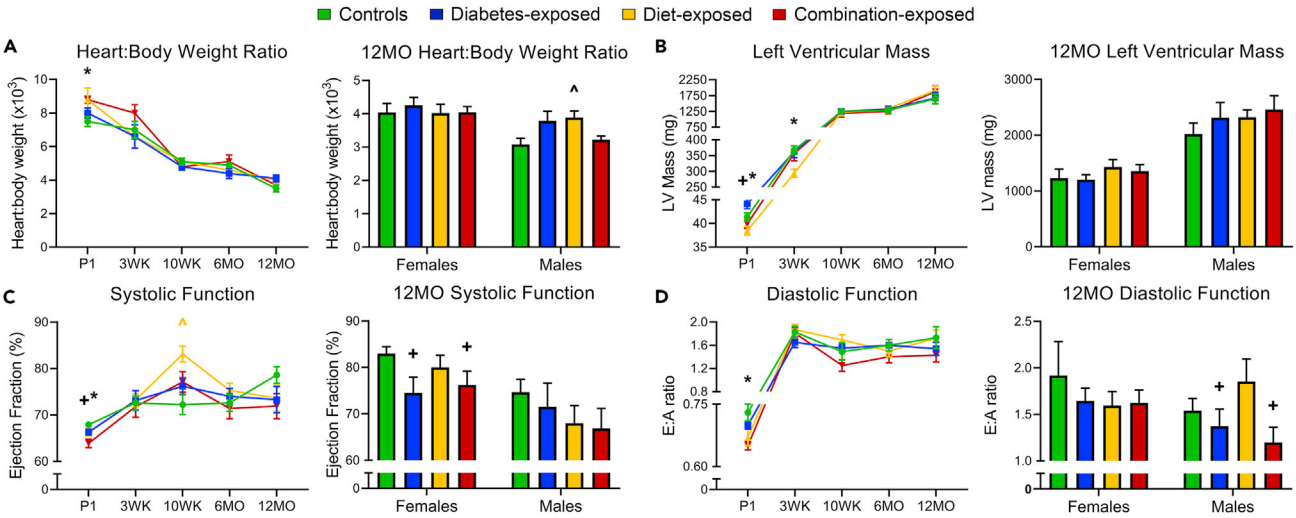

Figure 2. Exposed Offspring Are Born with Cardiomyopathy That Improves After Birth but Reemerges at 12MO

(A) Heart:body weight ratios over time with 12MO offspring separated by sex. N_{P1} = 216–250 offspring/group; N_{3WK} = 27–41; N_{10WK} = 21–35; N_{6MO} = 4–9; N_{12MO} = 15–20.

(B–D) LV mass (B), systolic function per ejection fraction (C), and diastolic function per E:A ratio (D) over time with 12MO offspring separated by sex. N_{P1} = 119–144 offspring/group; N_{3WK} = 18–30; N_{10WK} = 10–19; N_{6MO} = 17–28; N_{12MO} = 15–18.

Although not marked, heart:body weight and ejection fraction are both significantly higher in normal females than males, whereas LV mass is higher in males. Data represent mean ± SEM. $p \leq 0.05$: $^{+}$diabetes or *diet effect by two-way ANOVA, ^group effect by one-way ANOVA and Dunnett post-hoc test when interaction by two-way ANOVA.

See also Figure S1 and Table S3.

P1 to 12MO. Although smaller at birth, diet-exposed females gain more weight over time (p = 0.014). At P1, HF diet-exposed offspring have ~13% larger heart:body weight ratios than controls (Figure 2A). The difference is largely found in combination-exposed males and associated with higher mortality (Figure S1). Like in human infants born to diabetic mothers, cardiac mass normalizes after birth (El-Ganzoury et al., 2012; Garg et al., 2014; Hoodbhoy et al., 2019) with no apparent differences from 3WK to 6MO. In normal females, heart weight increases steadily up to 12MO, but diabetes-exposed females lose 20% of heart mass from 6 to 12MO (p = 0.019). In contrast, normal male heart mass increases until 6MO and then declines; diabetes- and diet-exposed male hearts continue to increase in mass from 6 to 12MO. This results in diet-exposed males having significantly larger heart:body weight ratios at 12MO. Left ventricular mass and cardiac function by echocardiography follow a similar pattern (Figures 2B–2D). As expected, both diastolic and systolic functions increase with growth. Control females and males have ~14% and 7% increases in ejection fraction, ~16% and 10% increases in shortening fraction, and 3- and 2-fold increases in E:A ratio (mitral valve flow velocity from early to late diastole) from P1 to 12MO, respectively, with the biggest changes from P1 to 3WK (Figure 2). Cardiac output increases 12- and 14-fold for females and males over a lifetime.

Both systolic and diastolic functions are poorer in diabetes- and diet-exposed P1 offspring (Figures 2C and 2D). Systolic function is more negatively affected by maternal HF diet in females and by maternal diabetes in males (Table S3). Diastolic function is poorer in diet-exposed newborns, especially females. Combination-exposed P1 offspring (of both sexes) have the poorest function, suggesting that dietary fat is a modifiable risk factor. Cardiac function improves after birth with no apparent differences until late adulthood. At 12MO, diabetes-exposed, but not diet-exposed females have poorer systolic function (Figure 2C) and males have poorer diastolic function (Figure 2D). Despite measurable differences in cardiac function, frank heart failure leading to differences in serum brain natriuretic peptide levels is not found (Table S2). As in previous studies (Baack et al., 2016), diet-exposed P1 offspring of both sexes have pulmonary hypertension (Table S3); this is not found in surviving offspring at later time points but may be confounded by early mortality. Overall, diabetes- and diet-exposed offspring have larger hearts and cardiac dysfunction at birth, intermediate improvement, and reemerging dysfunction in late adulthood. As shown below, the P1 and intermediate normalization correspond with initial improvement in bioenergetics (Figures 3 and 4); however, a second decline in bioenergetics at 6MO precedes cardiac dysfunction at 12MO.

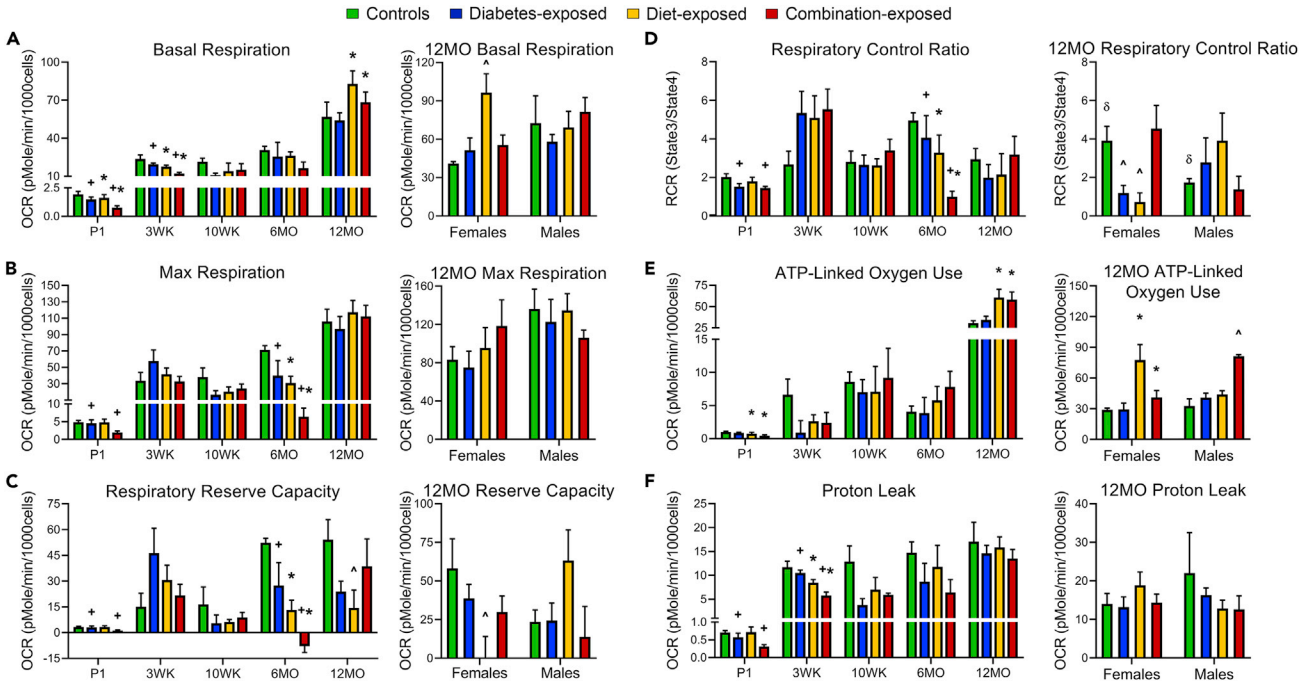

Figure 3. Diabetes- and HF Diet-Exposed Newborns Have Impaired Mitochondrial Respiration that Initially Improves but Reemerges at 6MO as Developmental Reliance on OXPHOS Increases.

(A–C) Basal (A), FCCP-stimulated maximal (B), and reserve (C) respiratory capacities over time with 12MO offspring separated by sex. Reserve capacity was calculated by subtracting basal from maximal respiration.

(D–F) Mitochondrial stress test was used to calculate respiratory control ratios (D), ATP-linked oxygen consumption (E), and mitochondrial proton leak (F) over time with 12MO offspring separated by sex.

Assay medium was supplemented with glucose and pyruvate. N_{P1} = 4–7 per group; N_{3WK} = 4–5; N_{10WK} = 3–4; N_{6MO} = 3; N_{12MO} = 7–11. Data represent mean ± SEM. $p \leq 0.05$: $^{+}$diabetes or *diet effect by two-way ANOVA, ^group effect by one-way ANOVA and Dunnett post-hoc test when interaction by two-way ANOVA, and $^{\delta}$sex-specific effect by Student's t test.

Metabolic Syndrome Does Not Explain Cardiac Disease in Aged Offspring Exposed to Maternal Glucolipotoxicity during Fetal Development

Offspring's metabolic phenotype is detailed in Figure 1 and Table S2. At birth, combination-exposed P1 offspring have higher whole-blood glucose levels (Figure 1E). Circulating TG and total and HDL cholesterol are not different between groups, whereas diet- but not diabetes-exposed P1 offspring have higher non-HDL cholesterol (Figure 1D; Table S2). Diabetes- and HF diet-exposed offspring have higher serum insulin and C-peptide levels (Figure 1F; Table S2) at birth with combination-exposed being the most affected with 2- to 4-fold higher levels. Diet-exposed offspring weigh less at birth, but diet-exposed females gain weight faster, catching up to peers at 3WK (Figure 1C). Past 3WK, adult males from all groups weigh more than group-matched females. By sex, weight is similar across groups at 10WK and 6MO, but by 12MO diet-exposed females weigh more than controls. This difference is not seen in males or diabetes-exposed offspring that develop cardiac dysfunction. Although neither fasting insulin nor euglycemic clamps were performed, our adult offspring do not appear to develop frank diabetes (blood glucose >200 mg/dL; Figure 1E), and glycated hemoglobin (HbA1c) levels are not different by sex or exposure (Figure 1F). On average, adult males have 2-fold higher TG than group-matched females (Figure 1D); this sex-specific difference reaches significance at 12MO ($p < 0.03$). By group, offspring have similar circulating lipids at 3WK. At 10WK, diabetes- and diet-exposed offspring have transiently higher serum TG levels (Figure 1D) that dissipate at 6 and 12MO. Offspring do not have evidence of fatty liver (Table S2). Adipocytokine levels (leptin or adiponectin) are similar until 6MO when diet-exposed, but not diabetes-exposed offspring develop transiently higher adiponectin levels (Table S2). This is not seen at 12MO. Neither renin nor soluble adhesion molecules (E-selectin and ICAM-1), known markers of vascular disease (Glowinska et al., 2005), are higher in exposed adult offspring. Overall, cardiac disease in diabetes-exposed adults is not explained by evidence of metabolic syndrome or markers of vascular disease. This suggests intrinsic cardiac pathology and supports our hypothesis that mitochondrial dysfunction plays a central role.

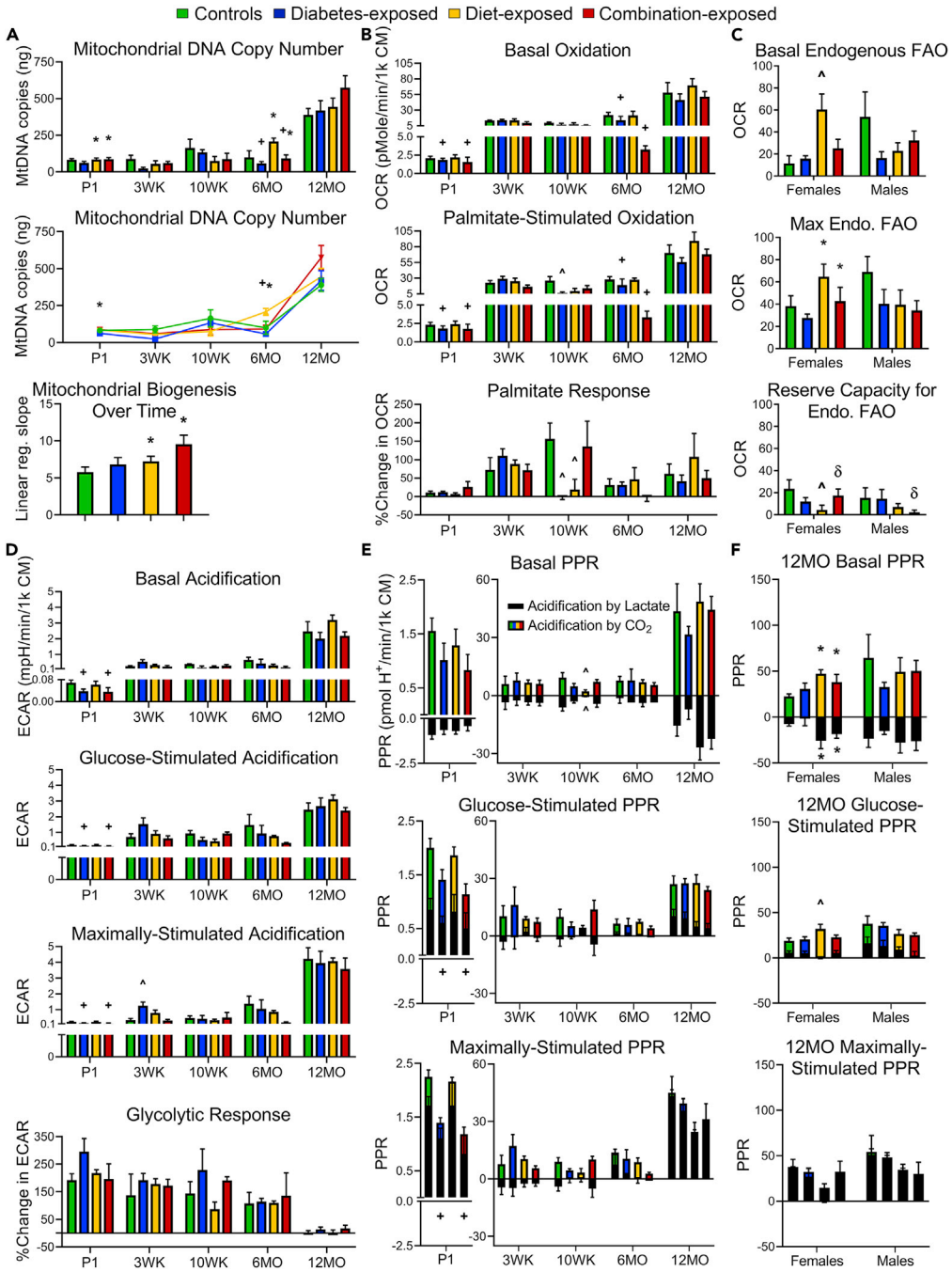

Figure 4. Mitochondrial Number, Basal Endogenous FAO, and Aerobic Glycolysis Increase with Age, but HF Diet Exposure Exaggerates Mitochondrial Biogenesis in Females, whereas Diabetes Exposure Incites Mitochondrial Dysfunction-Induced Biogenesis in Males causing Higher Oxygen Consumption and Poor Reserve Capacity in Aged Offspring

(A) Mitochondrial DNA copy number at each time point was used to estimate mitochondrial biogenesis from P1 to 12MO. N_{P1} = 10–15 per group; N_{3WK} = 4; N_{10WK} = 4; N_{6MO} = 3–4; N_{12MO} = 6–9.

(B) Basal OCR of CM in media without pyruvate, palmitate-stimulated OCR, and calculated responses to palmitate estimate FAO at each developmental time point.

(C) Basal, maximal, and reserve capacity for endogenous FAO at 12MO (Rogers et al., 2014).

Figure 4. *Continued*

(D–F) Basal, glucose-stimulated, and maximal extracellular acidification rates (ECAR) with cellular response to glucose (D) and proton production rates (PPR) over time (E) and at 12MO by sex (F). Maximal ECAR and PPR were stimulated with oligomycin in P1–6MO CM and with rotenone/antimycin A + monensin in 12MO CM.

N_{P1} = 4–7 per group; N_{3WK} = 4–5; N_{10WK} = 3–4; N_{6MO} = 3; N_{12MO} = 7–11 (B–F). Data represent mean ± SEM. $p \leq 0.05$: $^{+}$diabetes or *diet effect by two-way ANOVA, ^group effect by one-way ANOVA and Dunnett post-hoc test when interaction by two-way ANOVA, and $^{\delta}$sex-specific effect by Student's t test.

See also Figures S2 and S3.

Impaired Cellular Bioenergetics and an Exaggerated Age-Related Increase in Mitochondrial Number Precede Poorer Cardiac Function in Aged Offspring

Respiratory, fatty acid oxidation (FAO), and glycolytic capacities of primary CM from each exposure group were followed over time using extracellular flux analyses and are detailed in Figures 3, 4, and S2. Over the course of development, basal respiration and palmitate oxidation, respectively, increase 70- and 30-fold in control CM alongside a 5-fold increase in mitochondrial copy number. As in previous studies, diabetes-exposed P1 CM have lower basal, maximal, and reserve respiratory capacities (Figures 3A–3C), which translates to a lower respiratory control ratio (RCR; Figure 3D) (Mdaki et al., 2016a). Diet-exposed P1 CM also have lower basal respiration so that combination-exposed CM have the poorest respiratory capacity. After P1, prenatally exposed 3WK CM still have poorer basal respiration, but no differences remain by 10 weeks. With further maturation and increasing reliance on OXPHOS, 6MO diabetes- and diet-exposed CM have significantly lower maximal and reserve respiratory capacities than controls so that combination-exposed CM have a 5-fold lower RCR and little to no respiratory reserve. Importantly, impaired bioenergetics precede cardiac dysfunction at 12MO. Between 6MO and 12MO, there is an exaggerated increase in mitochondrial copy number (Figure 4A) so that 12MO diet-exposed CM have higher basal respiration and consume more oxygen to make ATP (Figures 3A and 3E). This is especially pronounced in diet-exposed females and combination-exposed males. Proton leak does not increase with mitochondrial number (Figure 3F), which suggests higher oxidative stress and risk of mitochondria-mediated cell death.

In line with respiration, diabetes-exposed P1 and 6MO offspring have impaired ability to oxidize palmitate (Figure 4B). In all groups, response to palmitate is the lowest at P1, and palmitate-stimulated oxidation steadily increases 30-fold from P1 to 12MO (Table S4). At 12MO, FAO is primarily of endogenous or stored lipids with minimal ability to increase with exogenous palmitate (Figures 4C and S2A). Diet-exposed female CM have higher basal and maximal endogenous FAO leaving little additional reserve capacity (Figure 4C). Conversely, diabetes- and diet-exposed male CM have lower endogenous FAO than group-matched females ($p = 0.001$), yet combination-exposed male CM have very little FAO reserve capacity. Although tissue staining does not detect differences in lipid droplet count between groups (Figures S3A–S3D), diet-exposed hearts of both sexes have lower expression of adipose differentiation-related protein, a lipid droplet-associated protein (Figure S3E), which correlates with less endogenous storage in this exposure group (Ueno et al., 2017). In females, this could be explained by depletion due to greater basal and maximal endogenous FAO (Figure 4C). Conversely, diabetes- and diet-exposed male CM have lower FAO than age-matched females ($p = 0.001$); paired with fewer stores and impaired FAO reserve capacity, findings suggest programmed perturbations in cardiac lipid metabolism.

Glycolysis is the primary ATP-generating pathway in the newborn heart. Here we demonstrate that glycolysis remains an important component of cardiac metabolism at all stages of development. Indeed, older CM have higher basal, glucose-stimulated, and maximal extracellular acidification rates (ECAR) than P1 CM. At 12MO, a relatively high rate of basal glycolysis limits response to additional glucose (Figure 4D). In line with previous findings, diabetes-exposed P1 CM have lower basal, glucose-, and oligomycin-stimulated ECAR (Mdaki et al., 2016a). With the exception of a transiently higher oligomycin-stimulated ECAR in diabetes-exposed 3WK CM, no group-related differences remain beyond P1. Group comparisons of maximal glycolysis in isolated CM over the course of development should be interpreted carefully. Through multiple validation steps, we found that oligomycin, which inhibits ATP synthesis by blocking the F0 subunit, results in maximal ECAR in newborn but not adult CM. The highest ECAR or maximal glycolytic capacity in adult rat CM is with rotenone/antimycin A respiratory complex inhibition combined with increased cellular ATP demands using monensin (Mookerjee et al., 2016) (Figure 4D). Indeed, 12MO rat CM have a poor ECAR response with glucose or oligomycin, but they do have spare anaerobic glycolytic reserve capacity under these conditions (Figure S2).

To fully interpret our glycolytic results, we calculated the proton production rates (PPR) to categorize lactate (anaerobic glycolysis) and CO_2 (aerobic respiration) contributions to ECAR (Mookerjee et al., 2017) (Figure 4E). In doing so, we confirmed previous findings that fetal exposure to diabetes impairs both anaerobic and aerobic glycolysis in P1 CM (Mdaki et al., 2016a). With oligomycin, anaerobic glycolysis remains lower in diabetes-exposed P1 CM. Beyond P1, basal and glucose-stimulated ECAR is primarily from aerobic respiration (CO_2). At 12MO, diet-exposed female CM have higher PPR from CO_2 than controls in both basal and glucose-stimulated conditions (Figure 4F); this is not surprising considering the higher number of mitochondria, basal oxygen consumption, and endogenous FAO in this group (Figures 3A, 4A, and 4C).

Exposed Offspring Have Sex-Specific and Fuel-Related Differences in Complex Function and Expression at P1 and 12MO Time Points

Using real-time extracellular flux analyses of permeabilized P1 and 12MO CM, we measured oxidation of individual fuels specific to complexes I, II, III, and IV (Figure 5A). Results, shown in Figures 5 and S4 and summarized in Table S5, highlight sex-specific differences in mitochondrial function with aging. In P1 CM, there are no sex-specific differences at baseline or with added complex fuels. At 12MO, permeabilized control male CM have higher OCR at baseline (Figure 5B), but females have greater response to pyruvate (I), palmitoyl-carnitine (I/III), and N,N,N′,N′-tetramethyl-p-phenylenediamine (TMPD)-ascorbate (IV) compared with group-matched males (Figures 5B and 5C), which suggests lower oxygen consumption at rest with greater reserve capacity that is intrinsic to mitochondrial function. Fetal exposure to maternal glucolipotoxicity lowers oxidation of complex I fuels in P1 CM from both sexes, but exposed females have lower pyruvate (I) and palmitoyl-carnitine (I/III) oxidation capacity (RCR), whereas exposed male CM have lower glutamine (I) oxidation capacity (Figure 5D). At 12MO, diet-exposed female permeabilized CM have higher basal OCR but lower responses to pyruvate (I), palmitoyl-carnitine (I/III), and succinate (II); diabetes-exposed 12MO females have lower oxidation capacity for duroquinol (III) (Figures 5B–5D). Interestingly, diabetes-exposed males have lower basal OCR but higher oxidative response to TMPD-ascorbate (IV) which may reflect relatively lower flow of electrons through complex I–III but retained ability to directly oxidize complex IV fuels, which requires more O_2 (Salabei et al., 2014).

Although differences in expression of complex proteins are present in exposed P1 offspring hearts of both sexes (Figure S4), they do not explain complex I dysfunction observed in permeabilized extracellular flux (XF) analyses. Regardless, findings emphasize the role of fetal sex in fuel-mediated cardiometabolic programming even at birth. By 12MO complex protein expression does not vary by sex as it did at P1, but diabetes-exposed female hearts have greater expression of SDHA (complex II) and COX5B (complex IV), and diet-exposed females have greater expression of NDUFA2 (complex I) (Figure 5E). For males, findings suggest that our model's bioenergetic phenotype is due to mechanisms other than complex protein expression. Taken together, permeabilized CM assays show higher O_2 consumption for ATP production in diet-exposed female and combination-exposed male CM by different sex-specific mechanisms and suggests that these groups are at higher risk for ROS production and the need for mitochondrial turnover to prevent mitochondria-mediated cell death.

Fetal Exposure and Sex Influence Physiologic Mitophagy in Aged Offspring CM

Previous work found that diabetes- and diet-exposed P1 CM have impaired mitochondrial dynamism and sex-specific differences in fission- and fusion-related protein activity that could confer cardioprotection to females (Larsen et al., 2019). Dynamism-related proteins also regulate mitophagy and mitochondria-mediated cell death (Dorn, 2019). To determine whether fetal exposure- or sex-related differences in mitochondria influence the risk of adult heart disease, we evaluated physiologic and stress-induced mitophagy in isolated 12MO CM. Using real-time confocal live-cell imaging, CM were stained with MitoTracker Green, Hoechst, and LysoTracker Red to quantify mitolysosomes (mitochondria co-localized with lysosomes) at baseline and their rate of formation following exposure to carbonyl cyanide-4-(trifluoromethoxy) phenylhydrazone (FCCP), a respiratory uncoupler that depletes MMP to drive mitophagy (Figure 6A; Video S1).

At baseline, there is no difference in the number of lysosomes (Figure 6B), but the number of co-localized mitolysosomes varies by group and sex (Figures 6A–6D). Diabetes-exposed CM have a higher number of mitolysosomes compared with controls (Figure 6C), which suggests a need for higher baseline physiologic mitophagy for mitochondrial quality control. Following FCCP-induced stress, all CM gain a measurable increase in mitolysosomes, but prenatal exposure influences the rate of formation. Diet-exposed CM have the lowest number of mitolysosomes at baseline, whereas the rate of formation following stress is

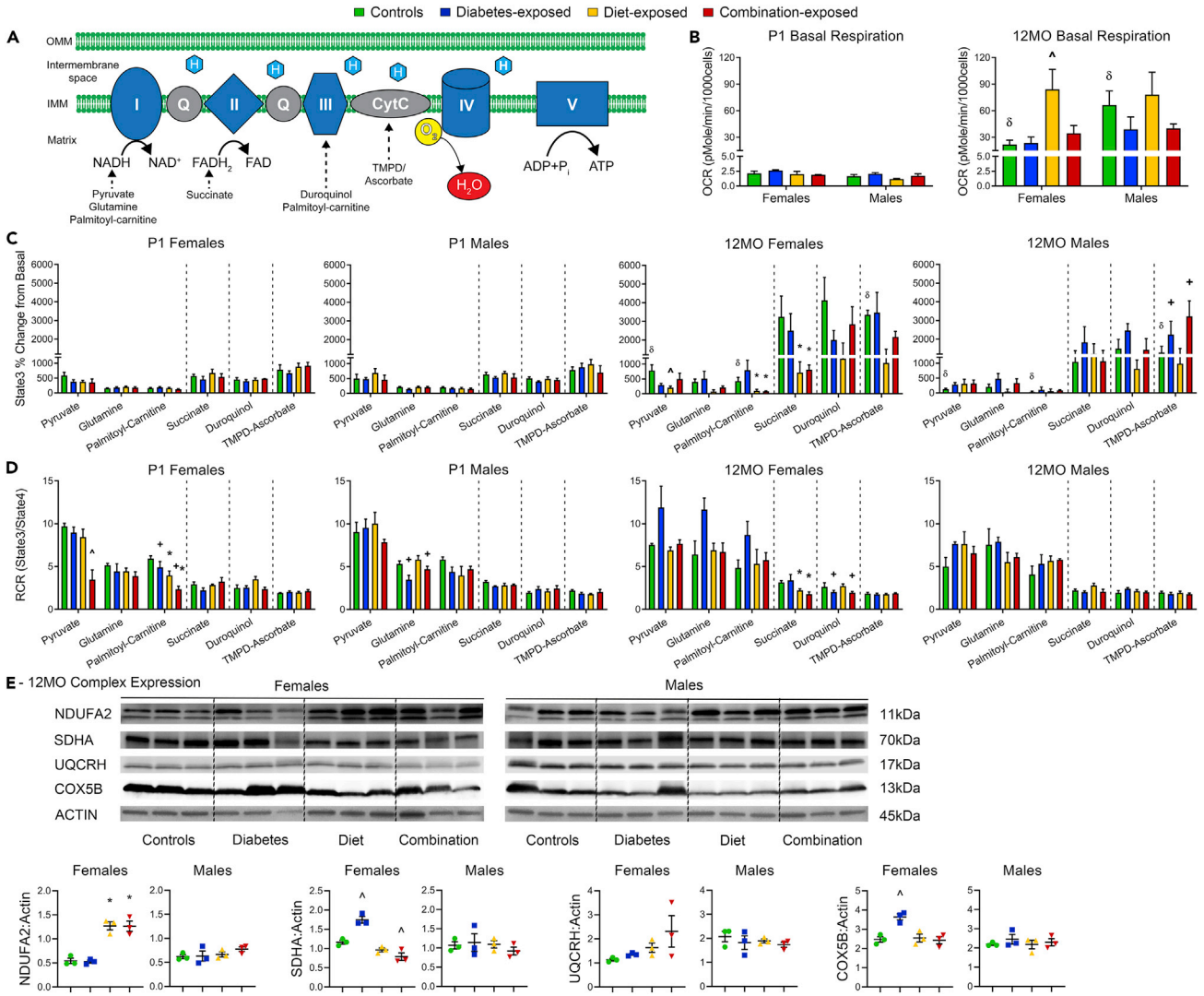

Figure 5. Diet-Exposed Females and Diabetes-Exposed Males Have Fuel-Specific Complex I Dysfunction at Birth and as OXPHOS Increases with Age Consume More Oxygen

(A) Schematic diagram of mitochondrial respiratory complexes and fuels feeding electrons into each. OMM, outer mitochondrial membrane; IMM, inner mitochondrial membrane.

(B) Basal oxygen consumption rates (OCR) of permeabilized P1 and 12MO CM.

(C) Oxidative responses to various complex fuels at P1 and 12MO time points by sex. State3 respiration (OCR) is shown as a percent change from basal OCR.

(D) Oxidation capacity per respiratory control ratios (RCR) at P1 and 12MO time points by sex. Dashed lines (C and D) separate fuels by complexes (I–IV).

(E) Relative expression of mitochondrial complex proteins in 12MO hearts by sex, normalized to beta-actin. For NDUFA2, lower (11kDa) band was used for analyses. Dashed lines separate exposure groups.

Data represent mean ± SEM. $p \leq 0.05$: $^{+}$diabetes or *diet effect by two-way ANOVA, ^group effect by one-way ANOVA and Dunnett post-hoc test when interaction by two-way ANOVA, and $^{\delta}$sex-specific effect by Student's t test. N_{P1} = 4–5 per group; N_{12MO} = 4–6.

See also Figure S4 and Table S5.

significantly faster (Figure 6E). Female and male offspring were analyzed separately. At baseline, control female CM have a higher number of mitolysosomes than males, which suggests higher rates of physiologic mitophagy for mitochondrial quality control than males; this supports previous findings at P1 (Larsen et al., 2019). Female and male CM from control offspring have similar rates of mitolysosome formation following metabolic stress. In females, diet-exposed CM have lower numbers of baseline mitolysosomes but a significantly faster rate of stress-induced mitophagy (Figures 6D–6E). In males, diabetes-exposed CM have higher numbers of baseline mitolysosomes, but low rates of stress-induced mitophagy. This is most

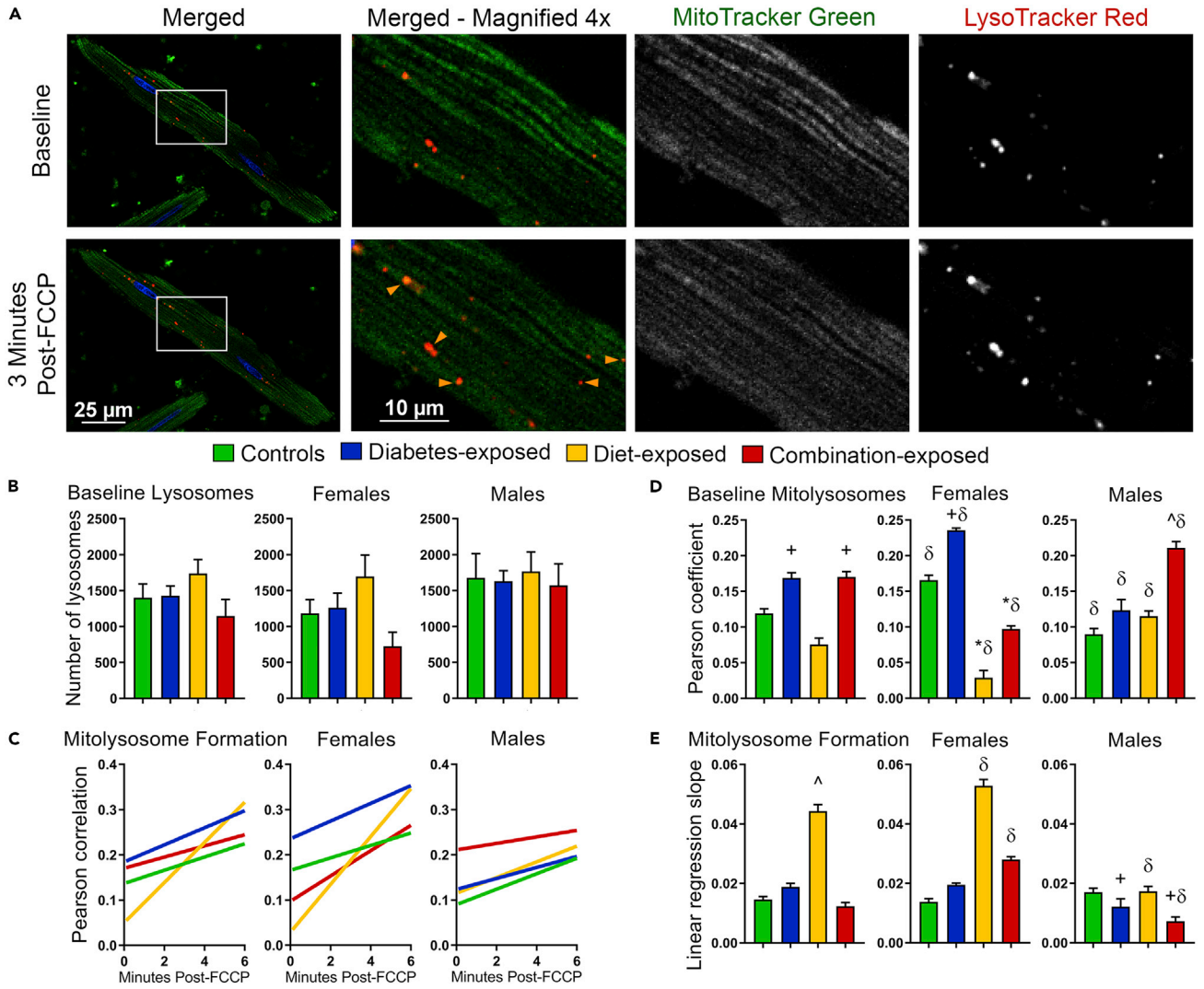

Figure 6. Baseline and Stress-Induced Mitophagy in 12MO CM Vary Significantly by Sex and Fetal Exposure

(A) Representative images of 12MO CM stained with MitoTracker Green, Hoechst, and LysoTracker Red. Once treated with FCCP, mitochondria lose their membrane potential and recruit lysosomes to undergo mitophagy. This is reflected by increasing number of co-localized mitochondria-containing autolysosomes (mitolysosomes) indicated by orange arrowheads (bottom row, middle-left image).

(B) Number of lysosomes at baseline, before FCCP treatment.

(C–E) Computer analyses of live video images quantified mitolysosome at baseline and over time (C) providing an estimate of physiologic (D) and stress-induced mitophagy after FCCP (E).

Data represent mean ± SEM (B and D–E) and linear regression of Pearson correlation coefficient over time (C). $p \leq 0.05$: $^{+}$diabetes or *diet effect by two-way ANOVA, ^group effect by one-way ANOVA and Dunnett post-hoc test when interaction by two-way ANOVA, and $^{\delta}$sex-specific effect by Student's t test. N = 7–11 offspring/group.

See also Video S1.

apparent in combination-exposed male CM and suggests impaired ability to further cull damaged mitochondria following metabolic stress (Figure 6E).

Diabetes-Exposed Male CM Have Faster MMP Loss and Mitochondria-Mediated Cell Death

Baseline and stress-induced rates of MMP loss and cell death were measured using confocal live cell imaging and high-content screening analyses of 12MO CM stained with MitoTracker Green, Hoechst, and TMRE, a marker of MMP (Figure 7A; Video S2). At baseline, there are no exposure-related differences in TMRE intensity, although diabetes-exposed CM trend lower (Figure S5A). Immediately after FCCP, CM from all groups lose 25% of their

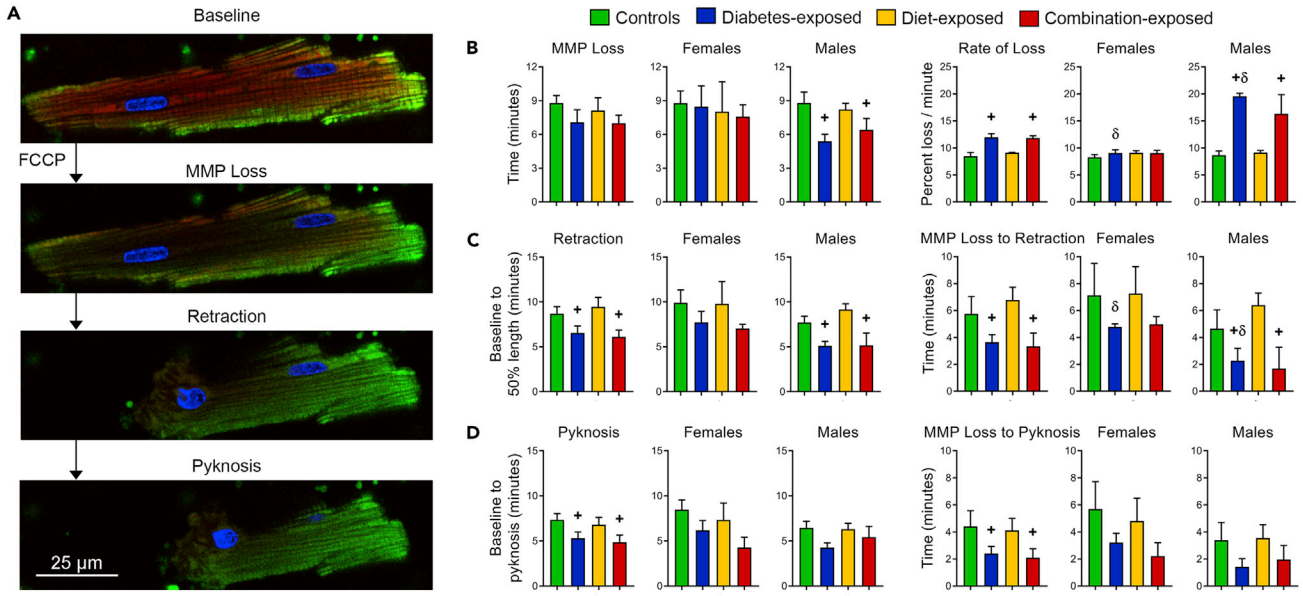

Figure 7. Diabetes-Exposed Male CM have Faster MMP Loss and Cell Death Following Metabolic Stress

(A) Representative images of 12MO CM stained with MitoTracker Green, Hoechst, and TMRE. Once treated with FCCP, mitochondria lose their MMP and trigger cell death as seen by retraction and pyknosis.

(B) MMP loss (75% from baseline) following FCCP-induced stress and the rate of MMP loss, calculated by linear regression analysis.

(C and D) Retraction and pyknosis, markers of CM death, were defined as the time from FCCP-induced stress to 50% original cell length (C) or to 10% loss in nuclear area (D), respectively. Time from start of MMP loss to either was calculated from a starting point of 25% MMP loss.

Data represent mean ± SEM. $p \leq 0.05$: +diabetes effect by two-way ANOVA, $^{\delta}$sex-specific effect by Student's t test. N = 8–11 offspring/group.

See also Figure S5 and Video S2.

MMP at similar rates; after this, diabetes-exposed male CM reach 50% and 75% loss faster than peers (Figure S5B). Thus, the linear rate of MMP loss is significantly faster in diabetes-exposed CM, particularly males (Figure 7B). There are no sex-specific differences in baseline TMRE intensity or rate of MMP loss in controls. However, diabetes-exposed males have a faster rate of MMP loss than group-matched females.

Stress-induced cell death was evaluated by two definitions: the time from FCCP to CM retraction (50% from baseline) or to pyknosis (Figure 7A). By both definitions, fetal exposure to maternal diabetes but not HF diet leads to faster cell death in 12MO CM (Figures 7C and 7D). The time from 25% MMP loss to retraction or pyknosis is also shorter in diabetes-exposed CM. Baseline cell length or width does not vary by exposure group but diabetes-exposed male CM are slightly longer at baseline compared with females (Figure S5A). Despite this, diabetes-exposed males have a shorter time from MMP loss to retraction compared with females ($p = 0.017$). Findings demonstrate that the risk of cardiac cell death following metabolic stress is greater in adult offspring exposed to diabetic pregnancy and that males are at the highest risk.

Expression of Mitochondria-Mediated Cell Death Regulators Varies by Sex

We have shown that P1 CM have impaired dynamism by sex-specific differences in fusion and fission proteins (Larsen et al., 2019). Here we compare expression of fission (DRP1, MFF, and MTFP1), fusion (MFN1, MFN2, and OPA1) and mitochondria-mediated cell death (VDAC, DAP3, and CYPD) proteins in 12MO offspring hearts to understand potential moderation of mitophagy and cell survival in adult CM (Dorn, 2019). Full results are shown in Figure S6, and sex-specific findings are listed in Table S6. Compared with females, male hearts had 2.8- to 3.8-fold lower expression of VDAC and 3- to 4-fold higher expression of CYPD. This finding, alongside lower physiologic mitophagy, suggests poorer mitochondria quality control and higher risk of mitochondria-mediated cell death by necrosis in males.

DISCUSSION

This study shows that offspring exposed to glucolipotoxicity during fetal development have mitochondrial dysfunction with disturbed cardiac bioenergetics across development, even when postnatal

influences are similar. Specifically, after birth as the heart increasingly relies on OXPHOS, bioenergetic disturbances result in exaggerated mitochondrial biogenesis, higher OCR, poor reserve capacity, and faster mitochondria-mediated CM death as aged adults. Findings confirm and build upon previous work showing mitochondrial dysfunction, cardiomyopathy, and higher mortality in exposed newborn offspring, and like humans, cardiac hypertrophy, dysfunction, and bioenergetics improve by weaning. However, impaired OXPHOS at 6MO precedes a functional decline in cardiac function at 12MO. This indicates a causal rather than a responsive change. Additionally, this study validates a reproducible and objective set of imaging studies to quantify baseline and FCCP-induced mitophagy alongside rates of mitochondria-mediated cell death. This "heart attack in a dish" assay shows that diabetes-exposed adult CM have faster MMP loss and mitochondria-mediated cell death under metabolic stress that could impart more cardiac damage following AMI. Our findings establish a role for mitochondria in myocardial programming and the fetal origin of adult heart disease that is outside secondary cardiovascular risks like metabolic syndrome or vascular disease.

Overall, findings add to mounting evidence that maternal glucolipotoxicity negatively impacts offspring's cardiac health into adulthood (Gao et al., 2016; Reynolds et al., 2013; Simeoni and Barker, 2009; Stuart et al., 2013), partially through programmed changes in mitochondrial function (Agarwal et al., 2018; Alfaradhi and Ozanne, 2011; Knudsen and Green, 2004; Shelley et al., 2009). While lasting mitochondrial consequences following fetal exposure to hyperglycemia or hyperlipidemia have been reported by others (Ferey et al., 2019; Gao et al., 2016; Mortensen et al., 2014; Theys et al., 2011), this study goes further to comprehensively evaluate individual and combined effects of fetal exposures on mitochondrial function as it relates to cardiac health over time. Following bioenergetic changes during maturation and aging confirms the increasing cardiac reliance on OXPHOS over time. To support this energetic demand, mitochondrial copy number increases over 5-fold from P1 to 12MO with the greatest rise between 6MO to 12MO. Importantly, at 6MO when normal hearts rely on OXPHOS and FAO for ATP generation (Goldberg et al., 2012; Lopaschuk and Dhalla, 2014), prenatally exposed offspring have impaired respiratory and FAO capacities. This leads to an exaggerated increase in mitochondrial copy number, which rises 5- to 7-fold in diet- and combination-exposed offspring, respectively. Given the combined data (mitochondrial copy number, basic bioenergetics assays, and permeabilized complex analyses), it is likely that prenatal exposures affect both the number and quality of mitochondria to influence cardiac risk over a lifetime. Authors propose that these exposure-related changes increase the risk of heart failure and cardiac damage from AMI in aged adults. This is supported by poorer diastolic function, faster MMP loss, and cell death under stress in diabetes-exposed adult males and poorer systolic function in diabetes-exposed females. By permeabilizing plasma membranes, mitochondrial complex function was evaluated independent of fuel transport and storage differences. Even then we found increased oxygen consumption and blunted responses to complex I fuels in 12MO diet-exposed female mitochondria. Taken together, limited fuel flexibility and depleted oxidative reserve capacities alongside age-related reliance on aerobic metabolism leaves little room for ATP production under ischemic conditions, such as AMI, which are reportedly higher in adults exposed to diabetic or obese pregnancy (Reynolds et al., 2013; Yu et al., 2019).

Mitochondrial function is an important component of ischemia-reperfusion injury (Maneechote et al., 2017). Excessive mitophagy leads to CM death and loss of cardiac contractility, both primary causes of cardiac damage and heart failure following AMI (Rosano et al., 2008). It is well-known that adults with long-standing diabetes suffer greater rates of diabetic cardiomyopathy and higher mortality from AMI (Peng et al., 2011). It is plausible that *in utero* exposures incite similar cardiac risks, and our study confirms lasting effects through mitochondria-mediated pathways. Although frank heart failure was not found, the faster stress-induced MMP loss and cell death in 12MO diabetes-exposed male CM may translate to more robust cardiac damage following increased energetic demands or AMI (Rosano et al., 2008). Although these consequences were not seen in diet-exposed offspring, their higher mortality rates (Figure 1) may have eliminated susceptible offspring. For this reason, we cannot conclude that functional and *in vitro* data represent all HF diet-exposed offspring rather than the least severely affected that survived to 12MO. Also, this may have contributed to the seemingly higher systolic function in 10WK diet-exposed offspring. Another explanation could be fatty acid-induced mitochondrial biogenesis contributing to a faster glycolytic-to-respiratory metabolic shift (Mdaki et al., 2016b), boosting cardiac contractility at 10WK but increasing oxidative stress and advancing "aging."

We also identified sex-specific differences in mitochondria that explain relative cardioprotection for females. We first identified sex-specific and exposure-related differences in dynamism at birth (Larsen et al., 2019), and here we report additional sex-specific differences in complex I fuel oxidation (Figure 5) and complex protein expression at P1 (Figure S4). These findings emphasize the role of fetal sex in fuel-mediated cardiac health, even as early as the perinatal period. We go further to describe programmed differences in respiration, complex fuel preference, and mitophagy in aged adults. Taken together, females appear to have better mitochondrial quality control mechanisms. Additionally, adult females are more negatively affected by fetal exposure to maternal HF diet, whereas males are more negatively affected by diabetes. If this translates to humans, dietary interventions could be clinically useful for personalized risk prevention. Finding both exposure- and sex-specific differences in bioenergetics and mitochondria-mediated cell death suggests that programmed mitochondrial dysfunction is caused by damage from adverse *in utero* conditions rather than maternal inheritance that would pass to both sexes alike. This is also supported by our model, which induces diabetes in the last one-third of pregnancy rather than prenatally.

To uncover additional mechanistic differences in cell death between sexes and exposure groups, we used immunoblotting of key regulatory proteins (Figure S6 and Table S6). VDAC is a central player in intrinsic apoptosis through apoptogen release, and overexpression induces apoptosis via mPTP opening, MMP dissipation, and cytochrome *c* release (Shoshan-Barmatz et al., 2017; Tomasello et al., 2009). Female hearts from all groups have higher VDAC expression than males. CYPD regulates MPT-driven necrosis by controlling mPTP opening (Porter and Beutner, 2018), and male hearts of all groups had higher CYPD expression than females. Ultimately, the higher VDAC expression alongside lower CYPD may confer cardioprotection in our female hearts; this pattern supports higher physiologic mitophagy and intrinsic apoptosis as the primary death pathway following FCCP. In contrast, lower VDAC and higher CYPD expression in male hearts supports MPT-driven necrosis as their primary route to cell death. Authors suspect this contributed to faster FCCP-induced cell death in diabetes-exposed male CM.

Strengths of our model include the ability to determine individual and combined effects of late-gestation diabetes and maternal HF diet on offspring. Litter size was normalized and offspring cross-fostered to normal dams to decrease confounding beyond prenatal exposures. Combination exposure allows us to determine whether prenatal glucolipotoxicity leads to more profound consequences than diabetes or diet alone. This is important clinically because the current treatment for diabetic pregnancy focuses on normalizing glucose but does not address hyperlipidemia or dietary fat intake (ACOG, 2013; Ryckman et al., 2015). Considering the higher rates of AMI in adult men (Millett et al., 2018), the higher baseline mitophagy alongside slower FCCP-induced cell death in normal females supports a cardioprotective role of physiologic mitophagy (Nah et al., 2017) and reflects superior mitochondrial quality observed in females (Cardinale et al., 2018; Ventura-Clapier et al., 2017). Studies using chemical compounds (Andres et al., 2014), preconditioning (Yuan and Pan, 2018), and caloric restriction (Abdellatif et al., 2018), all of which stimulate mitophagy, further support a cardioprotective role and give insight regarding preventative measures that could be used to improve life-long heart health. Although future studies are needed, we propose male and female differences in fuel-mediated programming are due to variable epigenetics (Gyllenhammer et al., 2020; Vijay et al., 2015), placental fuel transport (Jiang et al., 2017), hormonal influences (Groban et al., 2020; Rattanasopa et al., 2015), or a combination of these factors. Overall, our findings highlight sex as a strong biological variable that should be accounted for in DOHaD studies, especially when mitochondrial dysfunction is implicated.

Limitations of the Study

Mitochondrial findings are cardiac specific and should not be extrapolated to other tissues without further research. Although we evaluated many markers of cardiometabolic health over the course of development, this study did not directly examine hypertension or subclinical insulin resistance, which are reported in offspring of diabetic mothers (Agarwal et al., 2018; Alfaradhi and Ozanne, 2011; Dong et al., 2013). Regardless, cardiac findings in diabetes-exposed 12MO offspring (Table S2) could not be attributed to metabolic syndrome or circulating renin, adipocytokines, or soluble adhesion molecules. We further isolated myocardial findings by developing live-cell confocal imaging assays to objectively measure cellular responses to metabolic stress. Similar methods have been used to study mitochondria-mediated cell death by others (Elmore et al., 2001; Qi et al., 2016; Zhu et al., 2017), but our approach facilitates reproducible, quantitative, and adaptable methods to study mitophagy alongside rates of cell death. To overcome potential isolation-

induced stress, CM were seeded equally based on the number of live (not total) cells. Despite equal culture times, we cannot discount potential loss of more-stressed CM during incubation. However, we took care to measure baseline numbers of lysosomes, MMP, and cell length and width; there were only exposure-related differences after FCCP. Pyknosis is a well-known marker for both necrosis and apoptosis, however, binucleation and the sheer volume of mitochondria in adult cardiomyocytes (Page and McCallister, 1973) make it difficult to accurately grade chromatin distribution to distinguish apoptotic from necrotic pyknosis (Hou et al., 2016). For this reason and to further validate these methods, we included retraction, a morphologic marker of cardiomyocyte apoptosis (Kang et al., 2000). Retraction was a more sensitive measure in CM as it detected sex-specific differences, but this may not be true in all cell types.

Conclusions

In summary, this study shows that prenatal exposure to maternal diabetes increases the newborn and adult offspring's risk of mortality, impairs cardiac and bioenergetic function, and increases the risk of stress-induced cardiomyocyte death by sex-specific, mitochondria-mediated mechanisms. Considering the large number of infants born to mothers with diabetes and obesity, it is critical to confirm mechanisms and identify confounding factors so that pre- and postnatal prevention and intervention can be developed to improve long-term cardiac health in this growing population.

Resource Availability

Lead Contact

Further information and requests for resources should be directed to and will be fulfilled by the Lead Contact, Michelle L. Baack (Michelle.Baack@SanfordHealth.org).

Materials Availability

This study did not generate new unique reagents.

Data and Code Availability

The datasets generated and analyzed during the study are included within the manuscript body or Supplemental Information. All other data are available from corresponding authors upon request.

METHODS

All methods can be found in the accompanying Transparent Methods supplemental file.

SUPPLEMENTAL INFORMATION

Supplemental Information can be found online at https://doi.org/10.1016/j.isci.2020.101746.

ACKNOWLEDGMENTS

Authors thank the Sanford Histology and Imaging Core and Claire Evans and Kelly Graber for invaluable assistance with staining and confocal microscopy. We also thank the Sanford Animal Research Center, particularly Jennifer Agar, Kelsey Bush, and Brandon Whipple, for their skilled care and dedication to animal welfare. The study was supported by the National Institute of Children's Health and Disease (NIH-NICHD K08 HD078504), the Sanford Center for Pediatric Research (NIH-NIGMS CoBRE 2P20GM103620-06), the Sanford Center for Cancer Biology Research (NIH-NIGMS CoBRE P20GM103548), the National Center for Complementary and Integrative Health (NIH-NCCIH 1K01AT007826-01A1), and a National Science Foundation Sanford Program for Undergraduate Research (SPUR) training grant (NSF REU DBI-1262744).

AUTHORS CONTRIBUTION

M.L.B. is the principal investigator who conceived the study and with K.S.M. and E.J.L. developed methods. M.L.B. and E.J.L. designed and validated experiments, analyzed the data, and wrote the manuscript. E.J.L., T.D.L., T.C.T.G., and J.A.E. performed animal work, cardiomyocyte isolation, seahorse XF analyses, and serum and protein analyses. T.D.L acquired echocardiography, which was analyzed by A.L.W.. K.S.M., R.H.A., and J.T.C. helped develop, optimize, and validate imaging assays and HCS analyses methods. T.C.R. and K.A.K. performed maternal and offspring serum and liver lipid profiling. All authors assisted in experiments and contributed to development and review of this manuscript.

DECLARATION OF INTERESTS

The authors declare no competing interests.

Received: July 9, 2020
Revised: September 29, 2020
Accepted: October 24, 2020
Published: November 20, 2020

REFERENCES

Abdellatif, M., Sedej, S., Carmona-Gutierrez, D., Madeo, F., and Kroemer, G. (2018). Autophagy in cardiovascular aging. Circ. Res. *123*, 803–824.

ACOG (2013). Practice bulletin no. 137: gestational diabetes mellitus. Obstet. Gynecol. *122*, 406–416.

Agarwal, P., Morriseau, T.S., Kereliuk, S.M., Doucette, C.A., Wicklow, B.A., and Dolinsky, V.W. (2018). Maternal obesity, diabetes during pregnancy and epigenetic mechanisms that influence the developmental origins of cardiometabolic disease in the offspring. Crit. Rev. Clin. Lab. Sci. *55*, 71–101.

Alfaradhi, M.Z., and Ozanne, S.E. (2011). Developmental programming in response to maternal overnutrition. Front. Genet. *2*, 27.

Andres, A.M., Hernandez, G., Lee, P., Huang, C., Ratliff, E.P., Sin, J., Thornton, C.A., Damasco, M.V., and Gottlieb, R.A. (2014). Mitophagy is required for acute cardioprotection by simvastatin. Antioxid. Redox Signal. *21*, 1960–1973.

Ashrafian, H., Frenneaux, M.P., and Opie, L.H. (2007). Metabolic mechanisms in heart failure. Circulation *116*, 434–448.

Baack, M.L., Forred, B.J., Larsen, T.D., Jensen, D.N., Wachal, A.L., Khan, M.A., and Vitiello, P.F. (2016). Consequences of a maternal high-fat diet and late gestation diabetes on the developing rat lung. PLoS One *11*, e0160818.

Barbour, L.A. (2019). Metabolic culprits in obese pregnancies and gestational diabetes mellitus: big babies, big twists, big picture: the 2018 Norbert Freinkel award lecture. Diabetes Care *42*, 718–726.

Berezhnov, A.V., Soutar, M.P., Fedotova, E.I., Frolova, M.S., Plun-Favreau, H., Zinchenko, V.P., and Abramov, A.Y. (2016). Intracellular pH modulates autophagy and mitophagy. J. Biol. Chem. *291*, 8701–8708.

Bugger, H., and Abel, E.D. (2014). Molecular mechanisms of diabetic cardiomyopathy. Diabetologia *57*, 660–671.

Cardinale, D.A., Larsen, F.J., Schiffer, T.A., Morales-Alamo, D., Ekblom, B., Calbet, J.A.L., Holmberg, H.C., and Boushel, R. (2018). Superior intrinsic mitochondrial respiration in women than in men. Front. Physiol. *9*, 1133.

Cerf, M.E. (2018). Cardiac glucolipotoxicity and cardiovascular outcomes. Medicina *54*, 70.

Clausen, T.D., Mathiesen, E.R., Hansen, T., Pedersen, O., Jensen, D.M., Lauenborg, J., Schmidt, L., and Damm, P. (2009). Overweight and the metabolic syndrome in adult offspring of women with diet-treated gestational diabetes mellitus or type 1 diabetes. J. Clin. Endocrinol. Metab. *94*, 2464–2470.

Dong, M., Zheng, Q., Ford, S.P., Nathanielsz, P.W., and Ren, J. (2013). Maternal obesity, lipotoxicity and cardiovascular diseases in offspring. J. Mol. Cell Cardiol. *55*, 111–116.

Dorn, G.W., 2nd (2019). Evolving concepts of mitochondrial dynamics. Annu. Rev. Physiol. *81*, 1–17.

Dorn, G.W., 2nd, Vega, R.B., and Kelly, D.P. (2015). Mitochondrial biogenesis and dynamics in the developing and diseased heart. Genes Dev. *29*, 1981–1991.

El-Ganzoury, M.M., El-Masry, S.A., El-Farrash, R.A., Anwar, M., and Abd Ellatife, R.Z. (2012). Infants of diabetic mothers: echocardiographic measurements and cord blood IGF-I and IGFBP-1. Pediatr. Diabetes *13*, 189–196.

Elmore, S.P., Qian, T., Grissom, S.F., and Lemasters, J.J. (2001). The mitochondrial permeability transition initiates autophagy in rat hepatocytes. FASEB J. *15*, 2286–2287.

Ferey, J.L.A., Boudoures, A.L., Reid, M., Drury, A., Scheaffer, S., Modi, Z., Kovacs, A., Pietka, T., DeBosch, B.J., Thompson, M.D., et al. (2019). A maternal high-fat, high-sucrose diet induces transgenerational cardiac mitochondrial dysfunction independently of maternal mitochondrial inheritance. Am. J. Physiol. Heart Circ. Physiol. *316*, H1202–H1210.

Freinkel, N. (1980). Banting Lecture 1980. Of pregnancy and progeny. Diabetes *29*, 1023–1035.

Friedman, J.E. (2015). Obesity and gestational diabetes mellitus pathways for programming in mouse, monkey, and man—where do we go next? The 2014 norbert freinkel award lecture. Diabetes Care *38*, 1402–1411.

Galluzzi, L., Vitale, I., Aaronson, S.A., Abrams, J.M., Adam, D., Agostinis, P., Alnemri, E.S., Altucci, L., Amelio, I., Andrews, D.W., et al. (2018). Molecular mechanisms of cell death: recommendations of the nomenclature committee on cell death 2018. Cell Death Differ. *25*, 486–541.

Gao, L., Zhao, Y.-C., Liang, Y., Lin, X.-H., Tan, Y.-J., Wu, D.-D., Li, X.-Z., Ye, B.-Z., Kong, F.-Q., Sheng, J.-Z., et al. (2016). The impaired myocardial ischemic tolerance in adult offspring of diabetic pregnancy is restored by maternal melatonin treatment. J. Pineal Res. *61*, 340–352.

Garg, S., Sharma, P., Sharma, D., Behera, V., Durairaj, M., and Dhall, A. (2014). Use of fetal echocardiography for characterization of fetal cardiac structure in women with normal pregnancies and gestational diabetes mellitus. J. Ultrasound Med. *33*, 1365–1369.

Glowinska, B., Urban, M., Peczynska, J., and Florys, B. (2005). Soluble adhesion molecules (sICAM-1, sVCAM-1) and selectins (sE selectin, sP selectin, sL selectin) levels in children and adolescents with obesity, hypertension, and diabetes. Metabolism *54*, 1020–1026.

Goldberg, I.J., Trent, C.M., and Schulze, P.C. (2012). Lipid metabolism and toxicity in the heart. Cell Metab. *15*, 805–812.

Gregor, L., Remington, P.L., Lindberg, S., and Ehrenthal, D. (2016). Prevalence of pre-pregnancy obesity, 2011-2014. WMJ *115*, 228–232.

Groban, L., Tran, Q.-K., Ferrario, C.M., Sun, X., Cheng, C.P., Kitzman, D.W., Wang, H., and Lindsey, S.H. (2020). Female heart health: is GPER the missing link? Front. Endocrinol. *10*, 919.

Gustafsson, A.B., and Dorn, G.W., 2nd (2019). Evolving and expanding the roles of mitophagy as a homeostatic and pathogenic process. Physiol. Rev. *99*, 853–892.

Gyllenhammer, L.E., Entringer, S., Buss, C., and Wadhwa, P.D. (2020). Developmental programming of mitochondrial biology: a conceptual framework and review. Proc. R. Soc. B Biol. Sci. *287*, 20192713.

Heidenreich, P.A., Trogdon, J.G., Khavjou, O.A., Butler, J., Dracup, K., Ezekowitz, M.D., Finkelstein, E.A., Hong, Y., Johnston, S.C., Khera, A., et al. (2011). Forecasting the future of cardiovascular disease in the United States: a policy statement from the American Heart Association. Circulation *123*, 933–944.

Hollander, J.M., Thapa, D., and Shepherd, D.L. (2014). Physiological and structural differences in spatially distinct subpopulations of cardiac mitochondria: influence of cardiac pathologies. Am. J. Physiol. Heart circulatory Physiol. *307*, H1–H14.

Hoodbhoy, Z., Mohammed, N., Aslam, N., Fatima, U., Ashiqali, S., Rizvi, A., Pascua, C., Chowdhury, D., and Hasan, B.S. (2019). Is the child at risk? Cardiovascular remodelling in children born to diabetic mothers. Cardiol. Young *29*, 467–474.

Hou, L., Liu, K., Li, Y., Ma, S., Ji, X., and Liu, L. (2016). Necrotic pyknosis is a morphologically and biochemically distinct event from apoptotic pyknosis. J. Cell Sci. *129*, 3084–3090.

Jiang, S., Teague, A.M., Tryggestad, J.B., Aston, C.E., Lyons, T., and Chernausek, S.D. (2017).

Effects of maternal diabetes and fetal sex on human placenta mitochondrial biogenesis. Placenta *57*, 26–32.

Kang, P.M., Haunstetter, A., Aoki, H., Usheva, A., and Izumo, S. (2000). Morphological and molecular characterization of adult cardiomyocyte apoptosis during hypoxia and reoxygenation. Circ. Res. *87*, 118–125.

Knudsen, T.B., and Green, M.L. (2004). Response characteristics of the mitochondrial DNA genome in developmental health and disease. Birth Defects Res. C Embryo Today *72*, 313–329.

Kodde, I.F., van der Stok, J., Smolenski, R.T., and de Jong, J.W. (2007). Metabolic and genetic regulation of cardiac energy substrate preference. Comp. Biochem. Physiol. A Mol. Integr. Physiol. *146*, 26–39.

Krysko, D.V., Vanden Berghe, T., Parthoens, E., D'Herde, K., and Vandenabeele, P. (2008). Methods for distinguishing apoptotic from necrotic cells and measuring their clearance. Methods Enzymol. *442*, 307–341.

Kubli, D.A., and Gustafsson, Å.B. (2012). Mitochondria and mitophagy: the yin and yang of cell death control. Circ. Res. *111*, 1208–1221.

Larsen, D.T., Sabey, H.K., Knutson, J.A., Gandy, C.T., Louwagie, J.E., Lauterboeck, L., Mdaki, S.K., and Baack, L.M. (2019). Diabetic pregnancy and maternal high-fat diet impair mitochondrial dynamism in the developing fetal rat heart by sex-specific mechanisms. Int. J. Mol. Sci. *20*, 3090.

Lopaschuk, G.D., and Dhalla, N.S. (2014). Cardiac Energy Metabolism in Health and Disease (Springer).

Lopaschuk, G.D., and Jaswal, J.S. (2010). Energy metabolic phenotype of the cardiomyocyte during development, differentiation, and postnatal maturation. J. Cardiovasc. Pharmacol. *56*, 130–140.

Louwagie, E.J., Larsen, T.D., Wachal, A.L., and Baack, M.L. (2018). Placental lipid processing in response to a maternal high-fat diet and diabetes in rats. Pediatr. Res. *83*, 712–722.

Maneechote, C., Palee, S., Chattipakorn, S.C., and Chattipakorn, N. (2017). Roles of mitochondrial dynamics modulators in cardiac ischaemia/reperfusion injury. J. Cell. Mol. Med. *21*, 2643–2653.

Mdaki, K.S., Larsen, T.D., Wachal, A.L., Schimelpfenig, M.D., Weaver, L.J., Dooyema, S.D., Louwagie, E.J., and Baack, M.L. (2016a). Maternal high-fat diet impairs cardiac function in offspring of diabetic pregnancy through metabolic stress and mitochondrial dysfunction. Am. J. Physiol. Heart Circ. Physiol. *310*, H681–H692.

Mdaki, K.S., Larsen, T.D., Weaver, L.J., and Baack, M.L. (2016b). Age related bioenergetics profiles in isolated rat cardiomyocytes using extracellular flux analyses. PLoS One *11*, e0149002.

Millett, E.R.C., Peters, S.A.E., and Woodward, M. (2018). Sex differences in risk factors for myocardial infarction: cohort study of UK Biobank participants. BMJ *363*, k4247.

Mitra, K. (2013). Mitochondrial fission-fusion as an emerging key regulator of cell proliferation and differentiation. Bioessays *35*, 955–964.

Mookerjee, S.A., Gerencser, A.A., Nicholls, D.G., and Brand, M.D. (2017). Quantifying intracellular rates of glycolytic and oxidative ATP production and consumption using extracellular flux measurements. J. Biol. Chem. *292*, 7189–7207.

Mookerjee, S.A., Nicholls, D.G., and Brand, M.D. (2016). Determining maximum glycolytic capacity using extracellular flux measurements. PLoS One *11*, e0152016.

Mortensen, O.H., Larsen, L.H., Orstrup, L.K., Hansen, L.H., Grunnet, N., and Quistorff, B. (2014). Developmental programming by high fructose decreases phosphorylation efficiency in aging offspring brain mitochondria, correlating with enhanced UCP5 expression. J. Cereb. Blood Flow Metab. *34*, 1205–1211.

Murphy, E., Ardehali, H., Balaban Robert, S., DiLisa, F., Dorn Gerald, W., Kitsis Richard, N., Otsu, K., Ping, P., Rizzuto, R., Sack Michael, N., et al. (2016). Mitochondrial function, biology, and role in disease. Circ. Res. *118*, 1960–1991.

Nah, J., Miyamoto, S., and Sadoshima, J. (2017). Mitophagy as a protective mechanism against myocardial stress. Compr. Physiol. *7*, 1407–1424.

Ong, S.B., Kalkhoran, S.B., Hernandez-Resendiz, S., Samangouei, P., Ong, S.G., and Hausenloy, D.J. (2017). Mitochondrial-shaping proteins in cardiac health and disease - the long and the short of it! Cardiovasc. Drugs Ther. *31*, 87–107.

Page, E., and McCallister, L.P. (1973). Quantitative electron microscopic description of heart muscle cells. Application to normal, hypertrophied and thyroxin-stimulated hearts. Am. J. Cardiol. *31*, 172–181.

Peng, X.R., Zhao, Y.F., Zou, D.J., and Gu, P. (2011). [The role of diabetes mellitus as a risk factor of acute myocardial infarction]. Zhongguo Wei Zhong Bing Ji Jiu Yi Xue *23*, 322–328.

Perestrelo, T., Correia, M., Ramalho-Santos, J., and Wirtz, D. (2018). Metabolic and mechanical cues regulating pluripotent stem cell fate. Trends Cell. Biol. *28*, 1014–1029.

Pickles, S., Vigié, P., and Youle, R.J. (2018). Mitophagy and quality control mechanisms in mitochondrial maintenance. Curr. Biol. *28*, R170–R185.

Porter, G.A., Jr., and Beutner, G. (2018). Cyclophilin D, somehow a master regulator of mitochondrial function. Biomolecules *8*, 176.

Qi, Y., Qiu, Q., Gu, X., Tian, Y., and Zhang, Y. (2016). ATM mediates spermidine-induced mitophagy via PINK1 and Parkin regulation in human fibroblasts. Sci. Rep. *6*, 24700.

Rattanasopa, C., Phungphong, S., Wattanapermpool, J., and Bupha-Intr, T. (2015). Significant role of estrogen in maintaining cardiac mitochondrial functions. J. Steroid Biochem. Mol. Biol. *147*, 1–9.

Ren, Y., Zhou, Q., Yan, Y., Chu, C., Gui, Y., and Li, X. (2011). Characterization of fetal cardiac structure and function detected by echocardiography in women with normal pregnancy and gestational diabetes mellitus. Prenatal Diagn. *31*, 459–465.

Reynolds, R.M., Allan, K.M., Raja, E.A., Bhattacharya, S., McNeill, G., Hannaford, P.C., Sarwar, N., Lee, A.J., Bhattacharya, S., and Norman, J.E. (2013). Maternal obesity during pregnancy and premature mortality from cardiovascular event in adult offspring: follow-up of 1 323 275 person years. BMJ *347*, f4539.

Rogers, G.W., Nadanaciva, S., Swiss, R., Divakaruni, A.S., and Will, Y. (2014). Assessment of fatty acid beta oxidation in cells and isolated mitochondria. Curr. Protoc. Toxicol. *60*, 25.23.19–25.23.21.

Rosano, G.M., Fini, M., Caminiti, G., and Barbaro, G. (2008). Cardiac metabolism in myocardial ischemia. Curr. Pharm. Des. *14*, 2551–2562.

Ryckman, K.K., Spracklen, C.N., Smith, C.J., Robinson, J.G., and Saftlas, A.F. (2015). Maternal lipid levels during pregnancy and gestational diabetes: a systematic review and meta-analysis. BJOG *122*, 643–651.

Sacks, D.A., Hadden, D.R., Maresh, M., Deerochanawong, C., Dyer, A.R., Metzger, B.E., Lowe, L.P., Coustan, D.R., Hod, M., Oats, J.J., et al. (2012). Frequency of gestational diabetes mellitus at collaborating centers based on IADPSG consensus panel-recommended criteria: the Hyperglycemia and Adverse Pregnancy Outcome (HAPO) Study. Diabetes Care *35*, 526–528.

Salabei, J.K., Gibb, A.A., and Hill, B.G. (2014). Comprehensive measurement of respiratory activity in permeabilized cells using extracellular flux analysis. Nat. Protoc. *9*, 421–438.

Seo, B.J., Yoon, S.H., and Do, J.T. (2018). Mitochondrial dynamics in stem cells and differentiation. Int. J. Mol. Sci. *19*, 3893.

Shelley, P., Martin-Gronert, M.S., Rowlerson, A., Poston, L., Heales, S.J., Hargreaves, I.P., McConnell, J.M., Ozanne, S.E., and Fernandez-Twinn, D.S. (2009). Altered skeletal muscle insulin signaling and mitochondrial complex II-III linked activity in adult offspring of obese mice. Am. J. Physiol. Regul. Integr. Comp. Physiol. *297*, R675–R681.

Shoshan-Barmatz, V., Maldonado, E.N., and Krelin, Y. (2017). VDAC1 at the crossroads of cell metabolism, apoptosis and cell stress. Cell Stress *1*, 11–36.

Silveira, P.P., Portella, A.K., Goldani, M.Z., and Barbieri, M.A. (2007). Developmental origins of health and disease (DOHaD). J. Pediatr. *83*, 494–504.

Simeoni, U., and Barker, D.J. (2009). Offspring of diabetic pregnancy: long-term outcomes. Semin. Fetal Neonatal Med. *14*, 119–124.

Stuart, A., Amer-Wåhlin, I., Persson, J., and Källen, K. (2013). Long-term cardiovascular risk in relation to birth weight and exposure to maternal diabetes mellitus. Int. J. Cardiol. *168*, 2653–2657.

Theys, N., Ahn, M.T., Bouckenooghe, T., Reusens, B., and Remacle, C. (2011). Maternal malnutrition programs pancreatic islet mitochondrial

dysfunction in the adult offspring. J. Nutr. Biochem. *22*, 985–994.

Tomasello, F., Messina, A., Lartigue, L., Schembri, L., Medina, C., Reina, S., Thoraval, D., Crouzet, M., Ichas, F., De Pinto, V., et al. (2009). Outer membrane VDAC1 controls permeability transition of the inner mitochondrial membrane in cellulo during stress-induced apoptosis. Cell Res. *19*, 1363.

Ueno, M., Suzuki, J., Hirose, M., Sato, S., Imagawa, M., Zenimaru, Y., Takahashi, S., Ikuyama, S., Koizumi, T., Konoshita, T., et al. (2017). Cardiac overexpression of perilipin 2 induces dynamic steatosis: prevention by hormone-sensitive lipase. Am. J. Physiol. Endocrinol. Metab. *313*, E699–E709.

Upadhyaya, B., Larsen, T., Barwari, S., Louwagie, E.J., Baack, M.L., and Dey, M. (2017). Prenatal exposure to a maternal high-fat diet affects histone modification of cardiometabolic genes in newborn rats. Nutrients *9*, 407.

Ventura-Clapier, R., Moulin, M., Piquereau, J., Lemaire, C., Mericskay, M., Veksler, V., and Garnier, A. (2017). Mitochondria: a central target for sex differences in pathologies. Clin. Sci. *131*, 803–822.

Vijay, V., Han, T., Moland, C.L., Kwekel, J.C., Fuscoe, J.C., and Desai, V.G. (2015). Sexual dimorphism in the expression of mitochondria-related genes in rat heart at different ages. PLoS One *10*, e0117047.

Yu, Y., Arah, O.A., Liew, Z., Cnattingius, S., Olsen, J., Sorensen, H.T., Qin, G., and Li, J. (2019). Maternal diabetes during pregnancy and early onset of cardiovascular disease in offspring: population based cohort study with 40 years of follow-up. BMJ *367*, l6398.

Yuan, Y., and Pan, S.S. (2018). Parkin mediates mitophagy to participate in cardioprotection induced by late exercise preconditioning but bnip3 does not. J. Cardiovasc. Pharmacol. *71*, 303–316.

Zablah, J.E., Gruber, D., Stoffels, G., Cabezas, E.G., and Hayes, D.A. (2017). Subclinical decrease in myocardial function in asymptomatic infants of diabetic mothers: a tissue Doppler study. Pediatr. Cardiol. *38*, 801–806.

Zhu, M.-L., Lu, J.-X., Pan, G.-P., Ping, S., Zhao, F.-R., Qi, H.-T., Yu, H.-Y., Jian, X., Wan, G.-R., and Li, P. (2017). Traditional Chinese medicine Ka-Sai-Ping suppresses the growths of gastric cancers via induction of autophagy. Oncotarget *8*, 95075–95082.

iScience, Volume *23*

Supplemental Information

Age and Sex Influence Mitochondria and Cardiac Health in Offspring Exposed to Maternal Glucolipotoxicity

Eli J. Louwagie, Tricia D. Larsen, Angela L. Wachal, Tyler C.T. Gandy, Julie A. Eclov, Todd C. Rideout, Katherine A. Kern, Jacob T. Cain, Ruthellen H. Anderson, Kennedy S. Mdaki, and Michelle L. Baack

SUPPLEMENTAL FIGURES

Figure S1:

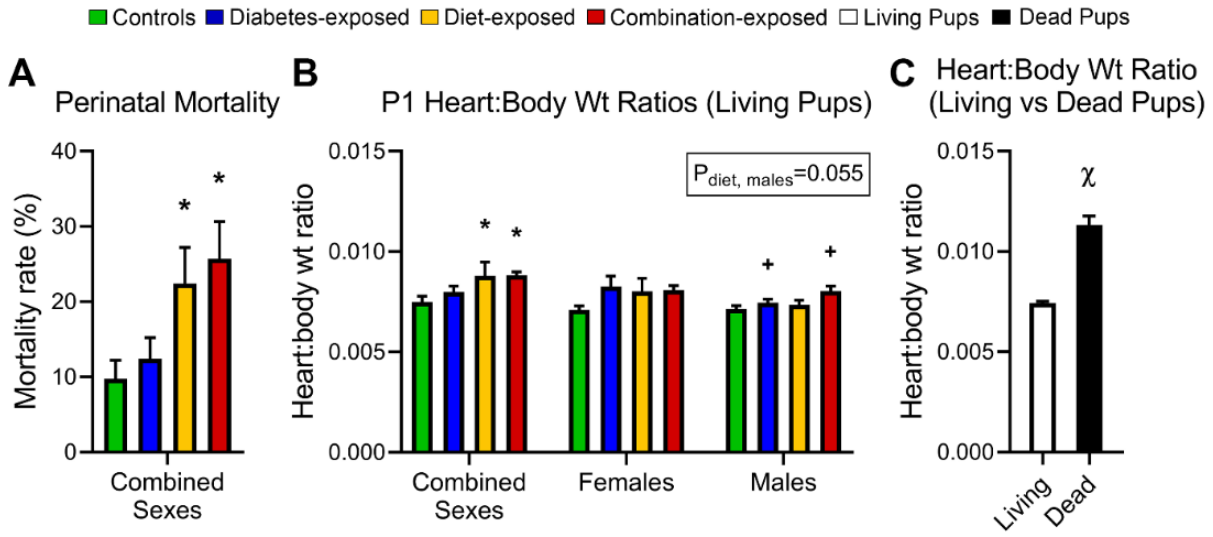

Figure S1: Perinatal mortality in exposed offspring is associated with significantly larger hearts, Related to Figures 1 and 2. **(A)** Perinatal mortality was calculated as: (litter size – live pups)/litter size x 100. N=20-26 litters/group. Litter size was confirmed by post-mortem evaluation of both uterine horns to count obvious placentation points, retained fetuses and dead P1 offspring as well as the number of live pups found in the cage. **(B)** Heart:body weight ratios of live P1 offspring with sexes combined and divided. N=216-243 offspring/group. **(C)** Heart:body weight ratios of both living and dead P1 offspring. N=257 living, 42 dead offspring. Data represent mean ± SE. $P \leq 0.05$: +diabetes or *diet effect by 2-way ANOVA, $^{\chi}$significant difference by Student's T-test.

Figure S2:

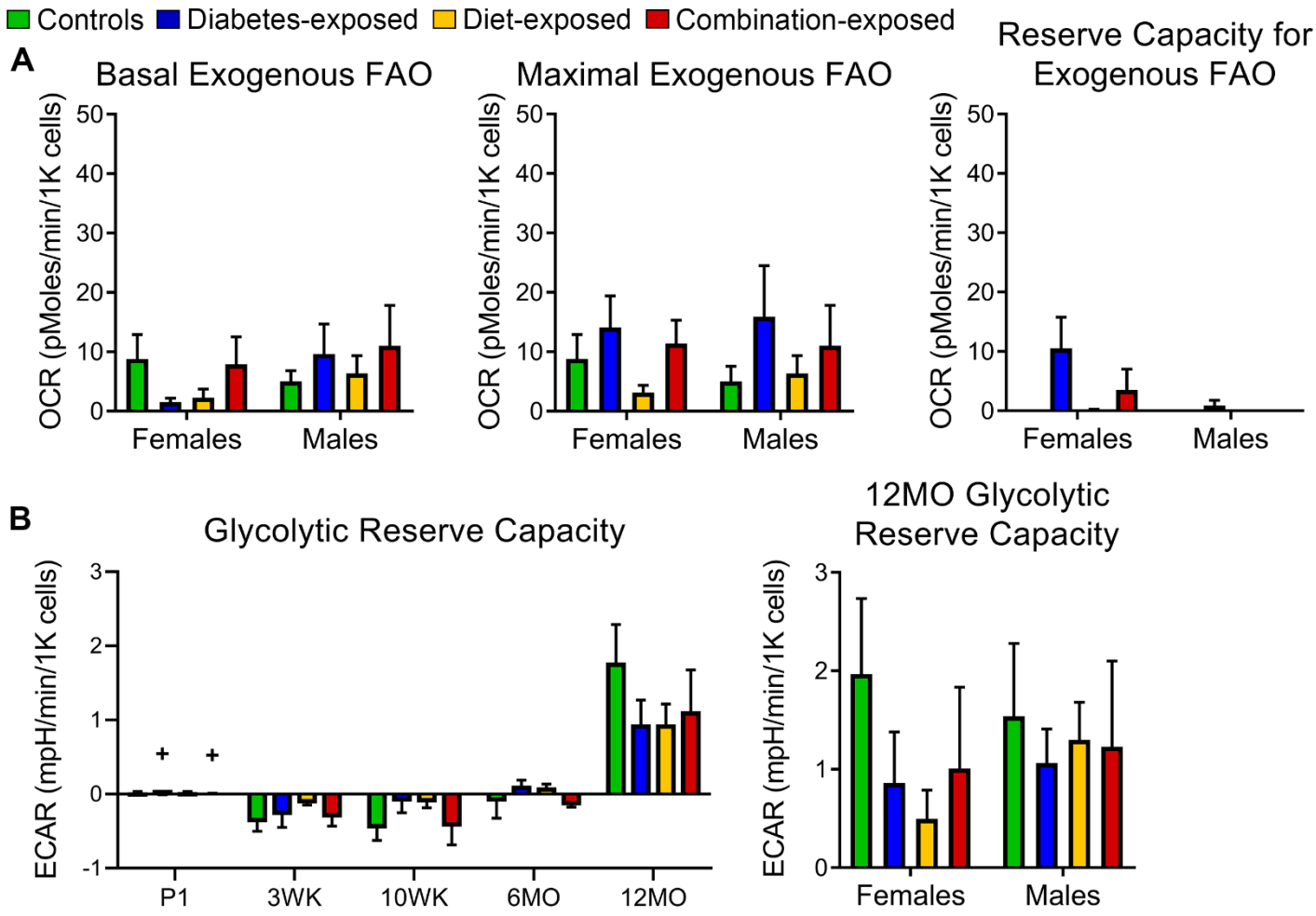

Figure S2: Supportive data for FAO and glycolysis, Related to Figure 4. (A) Basal (palmitate-stimulated OCR – basal endogenous OCR – OCR due to uncoupling by free FA), maximal (stimulated with FCCP), and reserve capacity (maximal – basal OCR) for exogenous FA oxidation at 12MO by sex; determined by the methods of (Rogers et al., 2014). Exogenous palmitate oxidation in 12MO cardiomyocytes is minimal relative to endogenous palmitate oxidation. N=8-11 per group. **(B)** Glycolytic reserve capacity over time with sexes separated at 12MO**.** Glycolytic reserve was calculated by subtracting the glucose-stimulated extracellular acidification rate (ECAR) from maximal ECAR. N_{P1}=4-7 per group; N_{3WK}=4-5; N_{10WK}=3-4; N_{6MO}=3; N_{12MO}=7-11. Data represent mean ± SE. $P \leq 0.05$: $^{+}$diabetes effect by 2-way ANOVA.

Figure S3:

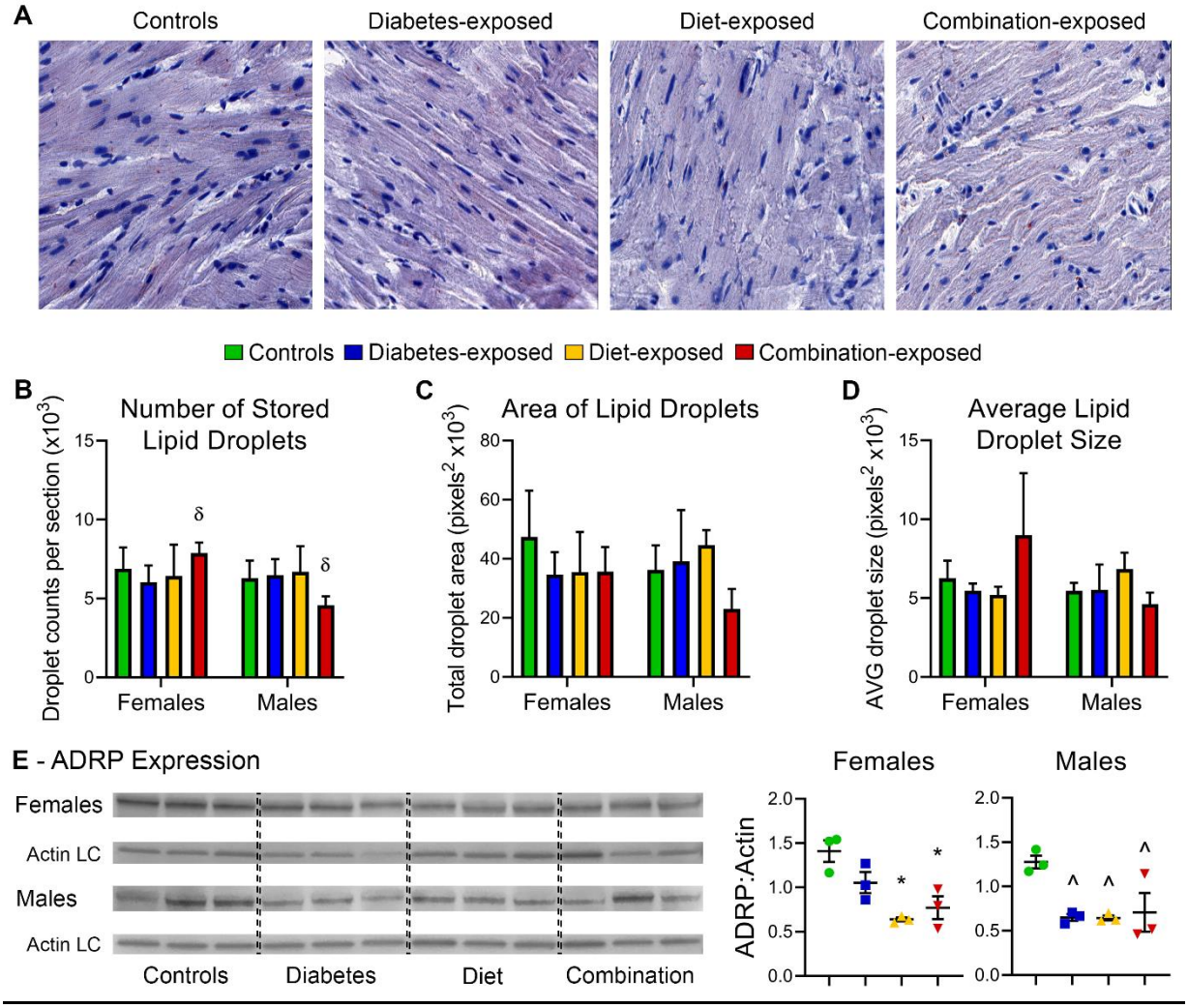

Figure S3: Differences in endogenous FAO levels may be related to altered lipid storage, Related to Figure 4. (A) Representative histological images of 12MO right ventricle sections (40x magnification) stained with Oil Red O and hematoxylin. Endogenous lipid droplets were quantified using Image J (NIH) to compare numbers of lipid droplets **(B)**, total area of droplets per section **(C)**, and average droplet sizes **(D)** from 12MO hearts by sex and exposure group. **(E)** As a surrogate marker for lipid droplets, Western blotting was used to determine relative expression of adipose differentiation-related protein (ADRP), a lipid-droplet coating protein that correlates with lipid deposition. Expression was normalized to the loading control (LC) β-actin. $N_{A\text{-}D}$=6-9; N_E=3 per sex per group. Data represent mean ± SEM. $P \leq 0.05$: $^{\delta}$sex-specific effect by 2-tailed Unpaired T-test.

Figure S4:

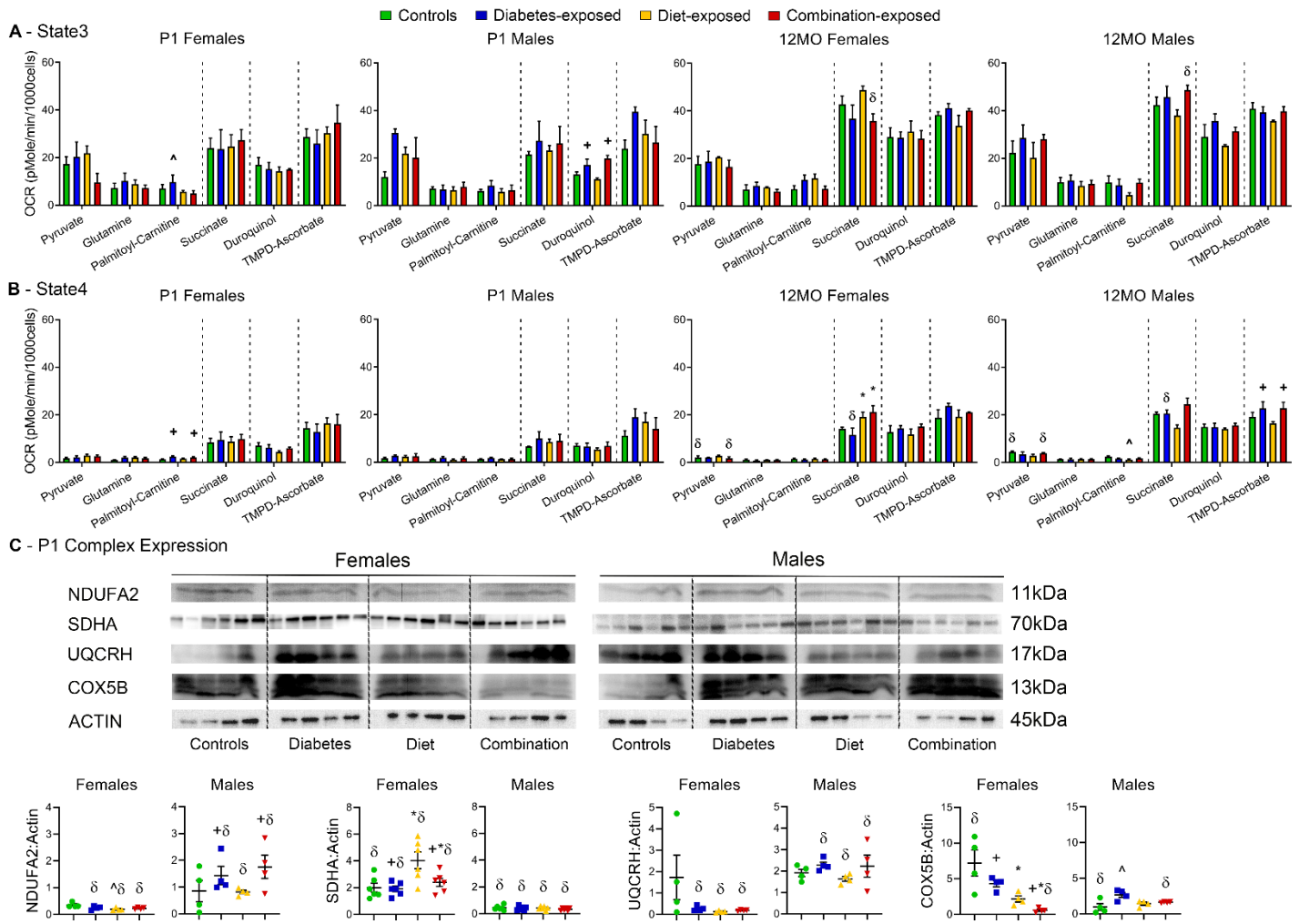

Figure S4: State3 and state4 respiration in permeabilized P1 and 12MO cardiomyocytes and complex protein expression in P1 hearts, Related to Figure 5. State3 **(A)** and state4 **(B)** respiration of permeabilized cardiomyocytes was used to calculate respiratory control ratios (RCR) for fuels feeding electrons to mitochondrial complexes I-IV. Dashed lines separate fuels by complexes. Western blotting was used to determine relative expression of electron transport chain complexes in P1 hearts by sex **(C)**. Expression on each blot was normalized to β-actin. Dashed lines separate groups. Data represent mean ± SEM. $P \leq 0.05$: $^{+}$diabetes or *diet effect by 2-way ANOVA, ^group effect by 1-way ANOVA and Dunnett post hoc test when interaction by 2-way ANOVA, and $^{\delta}$sex-specific effect by Student's T-test. For (A-B), N_{P1}= 4-5, N_{12MO} = 4-6 per sex per group; for (C), N= 4-6 per sex per group.

Figure S5:

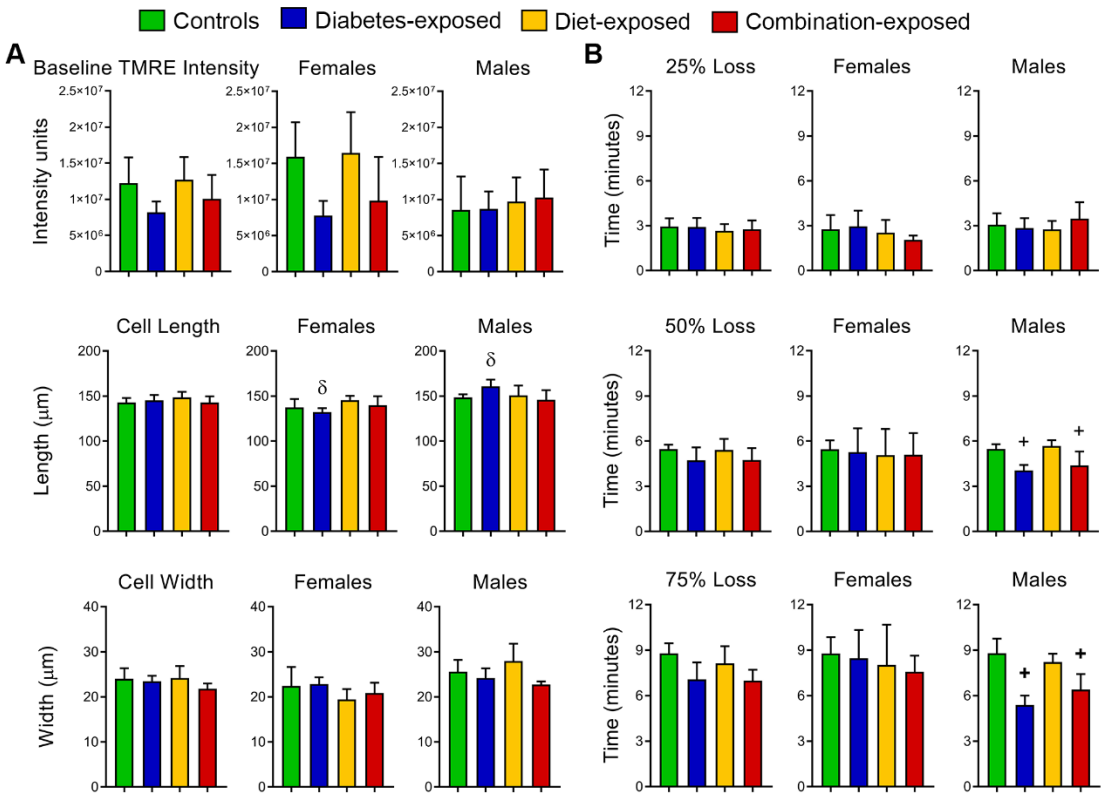

Figure S5: Baseline 12MO cardiomyocyte parameters and mitochondrial membrane potential (MMP) loss following FCCP, Related to Figure 7. (A) At baseline, there were no significant differences in TMRE fluorescent intensity, cell length, or cell width with the exception of diabetes-exposed males being longer than their female peers. **(B)** Following FCCP injection, CM lose up to 25% of their MMP at similar rates. Thereafter, diabetes-exposed male CM reach 50% and 75% loss at significantly faster rates than controls (p=0.015 and p=0.005, respectively). Data represent mean ± SEM. N=4-6 offspring/group per sex; N=8-11 animals/group for combined sexes. Significant differences ($p \leq 0.05$): $^{+}$diabetes effect by 2-way ANOVA, $^{\delta}$sex-specific effect by 2-tailed T-test.

Figure S6:

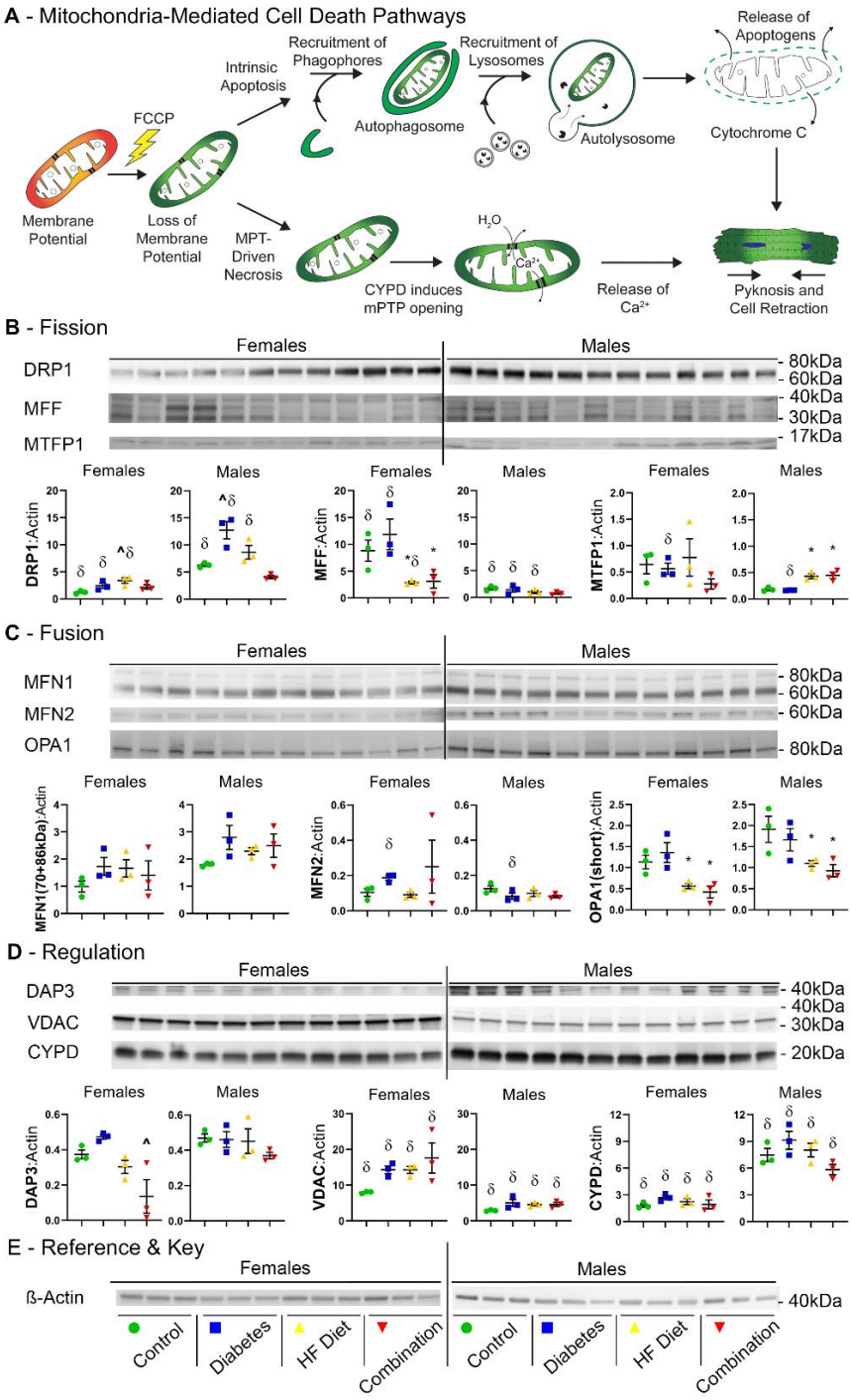

Figure S6: Expression of proteins involved in mitochondrial dynamism and mitochondria-mediated cell death in the adult offspring heart, Related to Results section "Expression of mitochondria-mediated cell death regulators varies by sex." (A) Pathways of mitochondria-mediated cell death. The ionophore uncoupler FCCP induces dissipation of the mitochondrial membrane potential, leading to increased mitophagy and cell death through two major mitochondria-mediated pathways: intrinsic apoptosis and mitochondrial permeability transition (MPT)-driven necrosis. In intrinsic apoptosis, mitochondria not degraded via mitophagy induce apoptosis through release of cytochrome C and other apoptogens. In MPT-driven necrosis, cyclophilin D (CYPD) induces necrosis via opening of the mitochondrial permeability transition pore. Western blots and densitometry analyses revealed exposure-dependent and sex-specific differences in **(B)** fission proteins (DRP1, MFF, and MTFP1), **(C)** fusion proteins (MFN1, MFN2, and OPA1), and **(D)** mitochondrial regulators of cell death (DAP3, VDAC, and CYPD) involved in these pathways. **(E)** Protein expression was normalized to loading control β-actin, and data points represent individuals from different litters. Ladder locations are marked on the right side of each immunoblot. Blot borders are delineated by black lines. Combined sexes analyses are not shown as intense sex-specific differences are apparent. Data represent mean ± SEM. N = 3 offspring/group per sex. Significant differences ($p \leq 0.05$): $^{\delta}$sex-specific effect by 2-tailed T-test with >2-fold expression difference, *diet effect by 2-way ANOVA, ^group effect significant by 1-way ANOVA and Dunnett's post hoc test when interaction was significant by 2-way ANOVA.

SUPPLEMENTAL TABLES

Table S1: Model maternal characteristics, Related to Figure 1.

Parameter	N/group	Controls (Mean±SE)	Diabetes-exposed (Mean±SE)	Diet-exposed (Mean±SE)	Combination-exposed (Mean±SE)	Diabetes (P value)	Diet (P value)	Interaction (P value)
Baseline weight, g		207±6	195±5	198±7	204±6	0.651	>0.999	0.176
Postdiet weight, g		240±3	233±4	***263±4**	***263±4**	0.490	**<0.0001**	0.358
Glucose, mg/dL		88±1	**+323±18**	106±11	**+313±15**	**<0.0001**	0.753	0.273
Ketones, mmol/L		0.43±0.03	**+0.55±0.04**	***0.50±0.04**	**+*0.64±0.05**	**0.001**	**0.041**	0.793
Insulin need, units	28-32	0±0	**+19±3**	0±0	**+22±3**	**<0.0001**	0.542	0.542
Serum TG, mg/dL	12-18	34±4	**+64±9**	***101±15**	**+*150±30**	**0.011**	**<0.0001**	0.542
NEFA, mg/dL		0.20±0.04	**+0.41±0.13**	***0.42±0.08**	**+*0.72±0.10**	**0.010**	**0.010**	0.660
TC, mg/dL		136.2±4.8	154.0±13.1	161.9±7.2	151.5±14.4	0.734	0.289	0.200
HDL, mg/dL		104.3±6.3	121.2±14.0	123.5±7.3	101.5±14.8	0.823	0.981	1.00
Non-HDL, mg/dL	5-7	31.9±6.6	32.8±3.6	***38.5±4.6**	***50.0±4.7**	0.226	**0.027**	0.296
Litter size, pups	23-26	11±1	12±1	10±1	11±1	0.230	0.230	>0.999

Significant differences ($p \leq 0.05$): $^{+}$diabetes or *diet effect by 2-way ANOVA. Maternal whole blood glucose, ketone levels, and insulin need were from gestational day (GD)15 to GD21. Maternal lipid levels were measured on postnatal day 1.

Table S2: Offspring characteristics over time, Related to Figure 1.

Age	Parameter	N/group	Controls (Mean±SE)	Diabetes-exposed (Mean±SE)	Diet-exposed (Mean±SE)	Combination-exposed (Mean±SE)	Diabetes (P value)	Diet (P value)	Interaction (P value)
P1[a]	Weight, g	216-250	6.2±0.1	6.2±0.1	***5.7±0.1**	***5.9±0.1**	0.114	**<0.0001**	0.291
	Glucose, mg/dL		77±1.3	74±1.4	81±0.0	**^85±3.6**	N/A	N/A	**0.049**
	Insulin, pmol/L	75-137	171.2±12.7	**+308.1±49.2**	***422.5±90.3**	**+*637.8±120.8**	**0.013**	**<0.0001**	0.581
	C-peptide, pmol/L		1293±81	1688±191	1285±111	**^2632±264**	N/A	N/A	**0.011**
	Serum TG, mg/dL	32-57	107.2±7.2	93.9±6.8	106.7±9.4	89.7±13.3	0.098	0.799	0.838
	Serum TC, mg/dL	3-7	63.0±8.7	62.3±6.7	72.9±6.5	65.2±5.1	0.609	0.437	0.669
	Serum HDL, mg/dL		12.4±3.5	11.6±1.4	11.5±2.4	9.8±2.0	0.636	0.604	0.853
	Serum non-HDL, mg/dL		38.7±3.2	50.6±5.8	**^67.9±1.6**	51.7±5.7	N/A	N/A	**0.024**
	Liver wt, g	4-8	0.21±0.02	0.24±0.02	0.21±0.02	0.17±0.01	0.805	0.096	0.096
	Liver TG, mg/dL		34.3±1.9	29.2±4.1	27.7±5.0	26.0±2.8	0.367	0.195	0.649
	Liver TC, mg/dL		16.1±0.6	14.3±1.2	13.7±0.5	14.4±0.5	0.557	0.203	0.163
3WK	Weight, g	27-41	67.8±2.2	70.2±4.1	68.9±3.4	**^55.3±3.5**	N/A	N/A	**0.012**
	Glucose, mg/dL		166±6.1	170±5.4	167±3.3	157±5.3	0.570	0.244	0.164
	Serum TG, mg/dL	14-24	63.2±6.9	74.0±7.6	63.5±8.6	96.6±23.3	0.079	0.355	0.370
	TC, mg/dL	6	124.2±9.5	107.6±6.5	124.0±11.2	124.1±7.9	0.367	0.372	0.362
	HDL, mg/dL		68.9±4.7	62.7±3.9	63.5±4.1	57.5±4.3	0.165	0.226	0.983
	Non-HDL, mg/dL	4-6	55.3±6.3	54.2±4.5	44.9±3.3	62.6±2.5	0.101	0.843	0.066
	Leptin, ng/mL	14-18	2.4±0.4	2.8±0.6	3.7±0.5	2.9±0.6	0.700	0.202	0.307
	Liver wt, g	4-8	2.98±0.24	3.07±0.15	2.65±0.10	2.61±0.30	0.907	0.072	0.761
	Liver TG, mg/dL		12.8±1.1	10.8±1.1	10.9±1.3	11.8±1.6	0.670	0.725	0.292
	Liver TC, mg/dL		16.0±0.8	16.0±0.7	15.0±0.5	16.0±0.8	0.502	0.451	0.511
10WK	Weight, g	21-35	286.6±9.7	279.4±10.3	265.0±13.0	270.6±16.3	0.947	0.205	0.589
	Glucose, mg/dL		129±4.6	158±14.8	132±7.5	117±2.5	N/A	N/A	**0.043**
	Serum TG, mg/dL	14-24	42.1±3.9	**^73.7±5.4**	**^76.9±13.3**	70.3±11.0	N/A	N/A	**0.026**
	TC, mg/dL	5-7	118.1±6.5	111.5±5.8	110.2±8.2	123.3±7.7	0.644	0.787	0.175
	HDL, mg/dL		63.9±4.9	63.3±2.4	57.4±5.9	55.0±6.4	0.770	0.164	0.860
	Non-HDL, mg/dL		54.2±4.3	50.0±5.6	52.8±3.8	61.4±6.3	0.660	0.332	0.214
	Leptin, ng/mL	12-24	2.1±0.4	1.5±0.2	1.8±0.4	1.5±0.3	0.153	0.733	0.583
	Renin, nM		0.12±0.01	0.10±0.01	***0.08±0.02**	***0.08±0.01**	0.448	**0.018**	0.456
	sE-Selectin, ng/mL		147.1±9.4	127.8±10.1	112.0±8.7	138.0±12.2	N/A	N/A	**0.037**

	sICAM-1, ng/mL		13.3±1.5	**+19.1±1.5**	***6.0±1.0**	**+*7.0±1.1**	**0.024**	**<0.0001**	0.107
	Liver wt, g		9.6±0.4	10.1±1.0	11.1±0.9	10.3±1.1	0.850	0.382	0.491
	Liver TG, mg/dL		5.3±0.3	4.3±0.6	5.1±0.9	6.0±0.3	0.958	0.153	0.077
	Liver TC, mg/dL	4-8	11.6±0.5	11.9±0.5	12.2±0.5	11.7±0.7	0.768	0.669	0.443
6MO	Weight, g		415.3±43.5	448.9±29.9	406.4±40.4	441.5±58.2	0.430	0.851	0.987
	Glucose, mg/dL	4-9	102±3.6	96±11.7	115±8.4	113±3.0	0.658	0.131	0.880
	Serum TG, mg/dL		97.8±8.7	105.8±9.6	105.6±8.4	110.3±17.3	0.583	0.592	0.885
	Adiponectin, ng/mL		31.4±3.0	30.1±3.7	**^33.4±1.8**	**^43.3±4.4**	0.209	**0.031**	0.106
	Renin, nM		42.8±3.0	49.5±5.2	35.3±2.5	41.3±2.8	0.082	0.063	0.828
	sE-Selectin, ng/mL		5.69±0.52	5.18±0.46	6.00±0.38	5.69±0.41	0.366	0.371	0.829
	sICAM-1, ng/mL	8-10	1.11±0.13	**+0.88±0.08**	0.96±0.09	**+0.79±0.05**	**0.035**	0.207	0.734
12MO	Weight, g		510.6±36.9	453.0±34.6	505.6±26.0	476.2±45.4	0.430	0.851	0.987
	Glucose, mg/dL	15-20	118±3.3	109±3.2	114±3.9	112±3.2	0.100	0.920	0.272
	HbA1c, %	8	7.54±0.45	7.95±0.70	7.51±0.32	6.81±0.30	0.760	0.224	0.248
	Serum TG, mg/dL	15-16	179.0±38.3	121.7±36.9	141.6±22.7	148.7±22.5	0.435	0.870	0.317
	Adiponectin, ng/mL		58.2±3.9	62.1±3.5	63.1±5.4	67.1±4.0	0.359	0.250	0.998
	Renin, nM		39.9±5.9	**+34.0±2.8**	***26.2±1.3**	**+*18.0±1.5**	**0.047**	**0.0001**	0.734
	sE-Selectin, ng/mL		5.1±0.5	5.2±0.3	5.9±0.7	6.0±0.8	0.897	0.162	0.915
	sICAM-1, ng/mL	8-10	2.1±0.7	1.5±0.2	1.4±0.2	1.6±0.4	0.543	0.464	0.349
	BNP, ng/mL	7-9	0.18±0.02	0.22±0.06	0.19±0.03	0.19±0.05	0.637	0.864	0.620

[a]P1 serum leptin levels have been previously published (Louwagie et al., 2018) and are not different between groups. P1, perinatal day one; WK, weeks; MO, months; N/A, not applicable; HbA1c, glycated hemoglobin; TG, triglycerides; TC, total cholesterol; HDL, high-density lipoprotein cholesterol; ICAM-1, intercellular adhesion molecule 1; BNP, brain natriuretic peptide. Significant differences ($p \leq 0.05$): [+]diabetes or *diet effect by 2-way ANOVA, ^group effect remained significant by 1-way ANOVA and Dunnett's post hoc test when interaction was significant by 2-way ANOVA.

Table S3: Sex-specific changes in cardiac structure and function over time, Related to Figure 2.

Age & Sex	Parameter	Controls (Mean±SE)	Diabetes-exposed (Mean±SE)	Diet-exposed (Mean±SE)	Combination-exposed (Mean±SE)	Diabetes (P value)	Diet (P value)	Interaction (P value)
P1 ♀	Heart:body wt ratio ($x10^{-3}$)	7.1±0.2	8.2±0.5	8.0±0.7	8.1±0.2	0.229	0.459	0.280
P1 ♂		7.1±0.2	**+7.5±0.2**	7.3±0.2	**+8.0±0.2**	**0.013**	0.055	0.361
P1 ♀	EF, %	68.6±0.8	67.8±0.7	***66.1±0.9**	***63.6±1.3**	0.080	**<0.001**	0.401
P1 ♂		67.4±0.8	**+64.2±0.8**	66.7±1.4	**+64.3±1.1**	**0.008**	0.770	0.663
P1 ♀	FS, %	37.2±0.6	36.6±0.6	***35.3±0.7**	***33.8±1.0**	0.147	**0.001**	0.560
P1 ♂		36.4±0.7	**+33.9±0.6**	35.9±1.1	**+34.4±0.9**	**0.012**	0.992	0.566
P1 ♀	CO, mL/min	5.8±0.1	6.0±0.2	***4.8±0.1**	***5.2±0.2**	0.081	**<0.001**	0.438
P1 ♂		5.5±0.1	**+5.9±0.2**	***4.8±0.1**	**+*5.4±0.2**	**0.002**	**<0.0001**	0.531
P1 ♀	E:A ratio	0.75±0.02	0.73±0.02	***0.65±0.02**	***0.52±0.02**	0.218	**<0.0001**	0.937
P1 ♂		0.72±0.02	0.68±0.02	0.70±0.03	0.68±0.01	0.195	0.772	0.607
P1 ♀	LV mass, mg	40.0±1.2	**+42.9±1.2**	***36.6±1.1**	**+*40.1±1.5**	**0.011**	**0.016**	0.797
P1 ♂		42.3±1.2	45.8±1.7	***40.7±1.6**	***39.6±1.0**	0.374	**0.005**	0.092
P1 ♀	IVSd, mm	0.57±0.01	0.58±0.01	0.55±0.01	0.56±0.01	0.350	0.168	0.939
P1 ♂		0.57±0.01	0.61±0.02	0.58±0.02	0.57±0.01	0.292	0.248	0.132
P1 ♀	PAAT:RVET ratio	0.28±0.01	0.27±0.01	***0.22±0.01**	***0.24±0.01**	0.407	**<0.0001**	0.287
P1 ♂		0.28±0.01	0.28±0.01	***0.23±0.01**	***0.25±0.01**	0.530	**<0.001**	0.294
3WK ♀	Heart:body wt ratio ($x10^{-3}$)	6.5±0.9	7.6±1.1	6.2±0.6	8.2±0.8	0.108	0.877	0.612
3WK ♂		7.9±0.7	5.6±0.9	6.9±1.2	7.8±0.8	0.462	0.505	0.092
3WK ♀	EF, %	73.7±1.8	78.4±2.3	72.9±1.9	75.3±3.7	0.156	0.422	0.636
3WK ♂		71.9±2.1	69.0±3.0	73.6±2.2	69.0±2.6	0.186	0.768	0.768
3WK ♀	FS, %	43.1±1.6	47.7±2.1	42.4±1.7	45.0±3.4	0.106	0.448	0.651
3WK ♂		42.1±2.0	39.8±2.3	42.1±1.9	39.2±2.2	0.194	0.932	0.747
3WK ♀	CO, mL/min	30.6±1.8	27.5±1.8	27.0±1.4	24.6±2.6	0.155	0.091	0.856
3WK ♂		31.8±2.2	27.8±1.8	29.2±1.9	26.6±2.9	0.170	0.430	0.757
3WK ♀	E:A ratio	1.92±0.18	1.57±0.09	1.84±0.08	1.98±0.19	0.460	0.230	0.078
3WK ♂		1.78±0.12	1.72±0.14	1.92±0.17	1.72±0.09	0.348	0.598	0.628
3WK ♀	LV mass, mg	367±21	319±19	**^286±14**	326±34	N/A	N/A	**0.043**
3WK ♂		367±17	400±25	305±25	382±31	0.052	0.159	0.432
3WK ♀	IVSd, mm	1.43±0.08	1.40±0.08	***1.21±0.07**	***1.23±0.11**	0.860	**0.029**	0.971
3WK ♂		1.39±0.05	1.62±0.09	1.33±0.10	1.49±0.09	0.079	0.212	0.882
3WK ♀	PAAT:RVET ratio	0.26±0.01	0.28±0.01	0.29±0.01	0.31±0.02	0.281	0.069	0.914
3WK ♂		0.30±0.02	0.33±0.02	0.29±0.01	0.30±0.02	0.199	0.300	0.750
10WK ♀	Heart:body wt ratio ($x10^{-3}$)	5.1±0.7	5.0±0.2	5.2±0.3	4.7±0.2	0.371	0.706	0.508
10WK ♂		5.2±0.3	4.6±0.4	4.8±0.5	4.8±0.2	0.437	0.868	0.456
10WK ♀	EF, %	72.9±2.5	77.7±3.7	**^83.7±2.0**	75.2±2.4	N/A	N/A	**0.043**
10WK ♂		69.7±3.3	75.2±1.6	***82.2±3.2**	***78.3±3.4**	0.782	**0.011**	0.113
10WK ♀	FS, %	43.6±2.3	48.8±3.9	**^54.4±2.5**	45.5±2.3	N/A	N/A	**0.039**
10WK ♂		41.4±2.7	45.9±1.4	***53.6±3.7**	***49.5±3.8**	0.937	**0.008**	0.125
10WK ♀	CO, mL/min	67.6±5.1	67.4±3.9	71.5±5.7	68.5±6.3	0.771	0.642	0.801
10WK ♂		83.8±4.7	92.0±5.7	102.0±9,9	87.6±6.9	0.657	0.315	0.106
10WK ♀	E:A ratio	1.52±1.16	1.41±0.07	1.69±0.11	1.35±0.18	0.095	0.669	0.407
10WK ♂		1.44±0.28	1.66±0.11	1.71±0.17	1.14±0.07	N/A	N/A	**0.048**
10WK ♀	LV mass, mg	980±96	1027±71.9	996±88	917±106	0.865	0.619	0.503
10WK ♂		1489±105	1415±63	1511±116	1374±153	0.333	0.930	0.769
10WK ♀	IVSd, mm	2.08±0.19	2.39±0.16	2.29±0.20	2.09±0.33	0.783	0.834	0.249
10WK ♂		2.40±0.17	2.35±0.11	2.48±0.18	2.35±0.17	0.573	0.809	0.787
10WK ♀	PAAT:RVET ratio	0.35±0.02	0.35±0.02	0.35±0.02	0.36±0.04	0.857	0.933	0.701
10WK ♂		0.37±0.02	0.36±0.01	0.34±0.03	0.32±0.03	0.369	0.068	0.756
6MO ♀	Heart:body wt ratio ($x10^{-3}$)	4.7±0.1	5.7±2.0	4.8±0.1	4.8±0.0	0.549	0.593	0.525
6MO ♂		5.1±0.2	4.3±0.3	4.4±0.2	5.2±0.4	N/A	N/A	**0.022**
6MO ♀	EF, %	74.4±1.8	79.0±2.1	76.9±2.1	70.6±2.9	N/A	N/A	**0.018**
6MO ♂		70.4±3.2	69.7±1.9	73.5±2.3	72.1±3.3	0.709	0.315	0.896
6MO ♀	FS, %	45.0±1.7	49.5±2.2	47.4±2.0	41.8±2.6	N/A	N/A	**0.022**
6MO ♂		42.2±2.8	41.2±1.5	44.8±2.2	43.6±2.8	0.647	0.302	0.974
6MO ♀	CO, mL/min	58.8±3.3	55.7±2.0	***67.1±4.7**	***62.9±4.6**	0.339	**0.049**	0.894

6MO ♂		69.9±6.5	80.1±3.7	85.5±4.4	78.2±6.2	0.743	0.224	0.095
6MO ♀	E:A ratio	1.65±0.12	1.64±0.14	1.47±0.14	1.40±0.14	0.730	0.125	0.749
6MO ♂		1.62±0.16	1.50±0.18	1.50±0.12	1.48±0.09	0.687	0.693	0.748
6MO ♀	LV mass, mg	1019±68	952±56	1062±59	971±65	0.238	0.643	0.858
6MO ♂		1591±153	1630±107	1639±124	1487±43	0.651	0.701	0.448
6MO ♀	IVSd, mm	2.0±0.1	2.2±0.1	1.9±0.1	2.0±0.1	0.266	0.551	0.768
6MO ♂		2.6±0.2	2.5±0.1	2.4±0.2	2.2±0.1	0.581	0.191	0.799
6MO ♀	PAAT:RVET ratio	0.41±0.02	0.35±0.03	0.40±0.02	0.39±0.03	0.227	0.582	0.293
6MO ♂		0.45±0.03	0.39±0.02	0.40±0.03	0.46±0.03	N/A	N/A	**0.035**
12MO ♀	Heart:body wt ratio ($x10^{-3}$)	4.0±0.4	4.3±0.3	4.0±0.3	4.0±0.2	0.601	0.611	0.667
12MO ♂		3.1±0.2	3.6±0.3	**^3.9±0.2**	3.3±0.1	N/A	N/A	**0.017**
12MO ♀	EF, %	83.0±1.5	**+74.5±3.4**	80.0±2.6	**+76.2±2.9**	**0.041**	0.833	0.424
12MO ♂		74.7±2.7	71.5±5.1	68.0±3.8	66.9±4.3	0.591	0.163	0.803
12MO ♀	FS, %	53.6±1.8	46.0±3.3	50.6±2.6	46.9±2.7	0.054	0.718	0.488
12MO ♂		45.9±2.7	44.0±4.3	40.3±3.0	39.5±3.6	0.696	0.148	0.869
12MO ♀	CO, mL/min	67.8±4.0	62.1±2.6	68.3±6.8	62.9±4.3	0.213	0.872	0.978
12MO ♂		77.1±5.1	87.8±7.7	86.7±7.2	87.3±7.1	0.407	0.505	0.457
12MO ♀	E:A ratio	1.9±0.4	1.6±0.1	1.6±0.2	1.6±0.1	0.591	0.454	0.508
12MO ♂		1.5±0.1	**+1.4±0.2**	1.9±0.2	**+1.2±0.2**	**0.031**	0.705	0.188
12MO ♀	LV mass, mg	1231±163	1204±90	1431±132	1359±117	0.699	0.174	0.862
12MO ♂		2021±198	2315±272	2325±130	2462±250	0.311	0.331	0.723
12MO ♀	IVSd, mm	2.4±0.2	2.1±0.1	2.7±0.2	2.5±0.2	0.172	0.071	0.664
12MO ♂		2.6±0.2	2.7±0.2	3.2±0.1	3.0±0.3	0.649	0.112	0.638
12MO ♀	PAAT:RVET ratio	0.61±0.04	0.60±0.03	0.48±0.04	0.62±0.07	0.141	0.265	0.119
12MO ♂		0.63±0.04	0.61±0.07	0.62±0.06	0.60±0.05	0.727	0.778	0.978

Cardiac function was assessed by echocardiography at all five time points for both sexes. For heart:body weight ratios, N_{P1}=216-250 offspring/group; N_{3WK}=27-41; N_{10WK}=21-35; N_{6MO}=4-9; N_{12MO}=15-20. For echocardiographic parameters, N_{P1}=119-144 offspring/group; N_{3WK}=18-30; N_{10WK}=10-19; N_{6MO}=17-28; N_{12MO}=15-18. ♀, females; ♂, males; P1, postnatal day one; WK, weeks old; MO, months old; EF, ejection fraction; FS, fractional shortening; CO, cardiac output; E:A ratio, mitral valve flow velocity from early:late diastole; LV, left ventricle; IVSd, interventricular septal thickness during diastole; PAAT, pulmonary artery acceleration time; RVET, right ventricular ejection time. Significant differences ($p \leq 0.05$): +diabetes or *diet effect by 2-way ANOVA, ^group effect significant by 1-way ANOVA and Dunnett's post hoc test when interaction was significant by 2-way ANOVA.

Table S4: Summary of age-related changes in offspring from birth (P1) to aged adulthood (12MO), Related to Figures 1-4.

Parameter	Normal development from P1 to 12MO	Exposure-related differences in females	Exposure-related differences in males
Weight gain	↑ 60-fold (females) and 100-fold (males)	Diet-exposed (but not combination-exposed) females gain more weight from P1 to 12MO	Not different from controls
Heart weight	↑ 34-fold (females) and 42-fold (males)	Diabetes-exposed females lose 20% of heart mass between 6MO to 12MO	Diabetes-exposed males gain 13% heart mass from 6MO to 12MO when controls plateau
LV mass by ECHO	↑ 31-fold (females) and 48-fold (males)	Diet-exposed females have more (~35-fold) LV growth from P1 to 12MO	Not different from controls
Systolic function	EF: ↑ 14% (females) and 7% (males) FS: ↑ 16% (females) and 10% (males)	Systolic dysfunction at birth resolves. Diabetes-exposed adult females have decline in EF and SF from 6MO to 12MO	Systolic dysfunction at birth improves. Diet-exposed males have EF and SF peak prematurely at 10WK
Diastolic function	E:A ratio: ↑ 3-fold (females) and 2-fold (males)	Diastolic dysfunction at birth resolves by 3WK, then not different from controls	Diastolic dysfunction at birth resolves. Diabetes-exposed adult males have decline in E:A from 6MO to 12MO
Cardiac output	↑ 12-fold (females) and 14-fold (males)	Not different from controls	Not different from controls
Basal respiration	↑ 70-fold	Rate of ↑ is higher in diet-exposed offspring, especially females from 6MO to 12MO	
Maximal Respiration	↑ 55-fold	Not different from controls	
ATP-linked oxygen consumption	↑ 60-fold	Rate of ↑ is higher in diet-exposed females and combination-exposed males (>100-fold)	
Basal acidification	↑ 70-fold	Rate of ↑ is lower in diabetes-exposed offspring (55-fold)	
Maximal acidification	↑ 20-fold	Not different from controls	
Palmitate oxidation	↑ 30-fold	Not different from controls	
mtDNA copy number	↑ 5-fold	Rate of ↑ is higher in diet-exposed offspring	

P1, postnatal day one; MO, months old; LV, left ventricle; ECHO, echocardiography; EF, ejection fraction; FS, fractional shortening; E:A ratio, mitral valve flow velocity from early:late diastole.

Table S5: Summarized changes in mitochondrial respiratory complex function, Related to Figure 5.

Age	Complex	Respiratory Control Ratio	Fuel Responses
P1	I	Lower in all exposed females Lower in diabetes-exposed males	No significant differences
	II	No significant differences	
	III		
	IV		
12MO	I	No significant differences	Lower in HF diet-exposed females Controls: females > males
	II	Lower in HF diet-exposed females	Lower in HF diet-exposed females Controls: trended (p=0.107) females > males
	III	Lower in diabetes-exposed females	Trended lower (p=0.073) in HF diet-exposed females Trended lower in diabetes-exposed (p=0.084) and HF diet-exposed (p=0.068) males
	IV	No significant differences	Trended lower (p=0.054) in HF diet-exposed females Higher in diabetes-exposed males Controls: females > males

Summary of changes in mitochondrial respiratory complex function following prenatal exposure to gestational diabetes and maternal high-fat (HF) diet.

Table S6: Sex-specific differences in 12MO cardiac protein expression, Related to Results section "Expression of mitochondria-mediated cell death regulators varies by sex."

Protein	Group	Females Mean±SE	Males Mean±SE	P value
DRP1	Controls	**1.22±0.16**	**6.28±0.24**	***<0.001**
	Diabetes-exposed	**2.42±0.49**	**12.74±1.61**	***0.004**
	Diet-exposed	**3.38±0.52**	**8.67±1.26**	***0.018**
	Combination-exposed	2.20±0.41	4.08±0.28	‡0.019
MFF	Controls	**8.82±1.98**	**1.68±0.25**	***0.023**
	Diabetes-exposed	**11.86±2.84**	**1.46±0.47**	***0.023**
	Diet-exposed	**2.85±0.24**	**1.01±0.28**	***0.007**
	Combination-exposed	3.10±1.25	0.71±0.14	0.130
MTFP1	Controls	0.64±0.18	0.18±0.02	0.060
	Diabetes-exposed	**0.56±0.11**	**0.16±0.00**	***0.020**
	Diet-exposed	0.77±0.35	0.43±0.05	0.391
	Combination-exposed	0.27±0.09	0.45±0.06	0.189
MFN1 (86kDa)	Controls	**0.06±0.01**	**0.21±0.02**	***0.002**
	Diabetes-exposed	**0.07±0.02**	**0.24±0.02**	***0.006**
	Diet-exposed	0.13±0.03	0.20±0.03	0.187
	Combination-exposed	0.11±0.06	0.22±0.04	0.241
MFN2 (70kDa)	Controls	0.10±0.02	0.13±0.02	0.478
	Diabetes-exposed	**0.19±0.01**	**0.08±0.02**	***0.010**
	Diet-exposed	0.09±0.01	0.10±0.02	0.741
	Combination-exposed	0.25±0.15	0.08±0.01	0.326
OPA1 (short band)	Controls	1.14±0.16	1.91±0.31	0.090
	Diabetes-exposed	1.36±0.24	1.66±0.26	0.439
	Diet-exposed	0.57±0.06	1.10±0.07	‡0.005
	Combination-exposed	0.42±0.14	0.93±0.14	0.065
DAP3	Controls	0.37±0.03	0.47±0.02	‡0.050
	Diabetes-exposed	0.47±0.01	0.46±0.04	0.808
	Diet-exposed	0.30±0.04	0.45±0.07	0.134
	Combination-exposed	0.14±0.10	0.37±0.02	0.074
VDAC	Controls	**7.98±0.17**	**6.28±0.24**	***<0.001**
	Diabetes-exposed	**14.33±1.07**	**12.74±1.61**	***0.003**
	Diet-exposed	**14.25±0.98**	**8.67±1.26**	***0.001**
	Combination-exposed	**17.58±4.23**	**4.08±0.28**	***0.038**
CYPD	Controls	**1.79±0.19**	**7.47±0.73**	***0.002**
	Diabetes-exposed	**2.68±0.23**	**9.13±1.00**	***0.003**
	Diet-exposed	**2.23±0.31**	**8.03±0.76**	***0.002**
	Combination-exposed	**1.94±0.50**	**5.83±0.56**	***0.007**
NDUFA2	Controls	0.54±0.06	0.54±0.06	0.342
	Diabetes-exposed	0.53±0.03	0.53±0.03	0.381
	Diet-exposed	1.27±0.09	1.27±0.09	‡0.004
	Combination-exposed	1.26±0.11	1.26±0.11	‡0.014
SDHA	Controls	1.63±0.05	1.07±0.09	0.426
	Diabetes-exposed	1.75±0.09	1.14±0.23	0.069
	Diet-exposed	0.96±0.05	1.09±0.10	0.290
	Combination-exposed	0.79±0.10	0.92±0.10	0.396
UQCRH	Controls	1.13±0.05	2.07±0.22	‡0.013
	Diabetes-exposed	1.35±0.04	1.82±0.28	0.181
	Diet-exposed	1.63±0.19	1.89±0.08	0.290
	Combination-exposed	2.31±0.65	1.74±0.11	0.433
COX5B	Controls	2.47±0.14	2.19±0.06	0.142
	Diabetes-exposed	3.64±0.16	2.45±0.25	‡0.016
	Diet-exposed	2.55±0.20	2.18±0.22	0.291
	Combination-exposed	2.43±0.19	2.30±0.19	0.638
ADRP	Controls	1.41±0.12	1.28±0.07	0.400
	Diabetes-exposed	1.05±0.12	0.65±0.04	‡0.032
	Diet-exposed	0.64±0.02	0.64±0.03	0.870
	Combination-exposed	0.77±0.13	0.71±0.22	0.816

Whole heart ventricle lysates from adult offspring were used to compare relative expression of proteins involved in mitochondrial fission, fusion, regulated cell death, complex expression, and lipid storage. Values were obtained by Western blotting and shown above as group mean ± SEM expression relative to β-actin. Sex-specific differences by T-test ($P<0.05$) are marked by boldface and *. Statistically significant differences ($P<0.05$) less than 2-fold different are instead marked by ‡. N = 3 males and 3 females/group.

TRANSPARENT METHODS

Experimental Animals

This study followed guidelines of The National Institutes of Health Guide for the Care and Use of Laboratory Animals and the Animal Welfare Act and was approved by the Sanford Institutional Animal Care and Use Committee (protocols 40-10-14B, 93-08-17B, and 131-06-20B). Facilities were temperature-controlled and light-dark cycled. Animals had free access to chow and water. Female Sprague Dawley rats (Envigo, Indianapolis, IN) were placed on either control diet (TD2018 Teklad, Envigo; 18% fat, 24% protein, 58% carbohydrates) or HF diet (TD95217 custom diet Teklad, Envigo; 40% fat, 19% protein, 41% carbohydrates) at least 28 days before breeding and throughout pregnancy. Females were bred with normal males fed control diet and monitored by vaginal swab for spermatozoa. Following ultrasound to confirm pregnancy on gestational day 14, dams received intraperitoneal injection of either citrate-buffered saline (Thomas Scientific, Swedesboro, NJ) diluent or 65mg/kg streptozotocin (Sigma-Aldrich, Inc., St. Louis, MO) to induce diabetes. Thereafter, dams were partially treated with twice-daily sliding scale insulin (regular and glargine, Eli Lilly and Co., Indianapolis, IN) to keep blood glucose levels at 200-400mg/dL. Tail-nick whole blood sampling was done to measure ketones and blood glucose (Precision Xtra ketone meter and glucometer, Abbott Laboratories, Abbott Park, IL). Dams not manifesting diabetes (blood glucose >200mg/dL) within 48 hours were excluded from this study. While maternal diabetes was induced by pancreatic damage, the developing offspring were consistently exposed to maternal hyperglycemia, hyperlipidemia and fetal hyperinsulinemia in the last 1/3 or pregnancy (Baack et al., 2016; Louwagie et al., 2018; Mdaki et al., 2016a) (Tables S1 and S2).

Dams delivered spontaneously to yield offspring of both sexes from four distinct groups: controls, diabetes-exposed, HF diet-exposed, and combination-exposed as previously described in detail (Louwagie et al., 2018; Mdaki et al., 2016a; Mdaki et al., 2016b; Upadhyaya et al., 2017). Litter size included live and dead pups as defined by counting the number of live and dead pups in the cage alongside direct uterine examination to count placentations, resorptions, or retained stillborns in each uterine horn. Perinatal mortality was calculated as: (litter size – live pups)/litter size x 100. On P1, litter size was equalized (8 pups/dam) and offspring were cross-fostered to normal timed pregnant dams fed a control diet and delivering 0-7 days prior to corresponding experimental offspring. To ensure that exposure to diabetes and/or diet was only prenatal, all pups were weaned to a control diet before being aged to preset time points (3WK, 10WK, 6MO, or 12MO). At all five time points, hearts were collected under 5% isoflurane anesthesia and immediately used to isolate primary ventricular cardiomyocytes (CM) or snap frozen in liquid nitrogen and stored at -80ºC.

Isolation of Primary Cardiomyocytes

Primary ventricular CM were isolated from offspring as previously described (Mdaki et al., 2016b). In brief, newborn (P1) hearts were collected immediately following euthanasia and transferred to Hank's Balanced Salt Solution (HBSS) on ice. Atria were removed before mincing ventricles. Ventricular pieces were digested via 5-6 alternating cycles of: 1) stirring for 5 min at 50rpm in 0.1% trypsin with 0.02% DNase I (in 0.15M NaCl), and 2) trituration at 1-2mL/sec for 5 min. Trypsin/DNase I mix was deactivated with bovine serum before centrifuging cells at 1600rpm at 22C for 10 min (centrifuge: Eppendorf Centrifuge 5810 R). Cell pellets were resuspended in DMEM-1 (DMEM supplemented with 10% BS and 1% penicillin/streptomycin) with 0.0002% DNase I, seeded to uncoated 35mm dishes, and incubated for 1 hr in humidified 37C, 5% CO_2 to allow fibroblast attachment. CM were then gently detached, resuspended in DMEM-1, and counted with Trypan Blue and hemocytometer before seeding to 0.1% gelatin-coated Seahorse XF24 V7 PS cell culture microplates at 150,000 viable CM/well for Extracellular Flux Analyses (see below) or at 40,000 CM/well for Permeabilized Extracellular Flux Analyses (see below). CM were allowed to adhere overnight (12-16 hr) before experimentation.

To isolate CM from 3WK, 10WK, 6MO, and 12MO offspring, following euthanasia hearts were placed in Perfusion Buffer (PB; 120.4mM NaCl, 14.7mM KCl, 0.6mM KH_2PO_4, 0.6mM Na_2HPO_4, 1.2mM $MgSO_4$-$7H_2O$, 10mM HEPES, 4.6mM $NaHCO_3$, 30mM taurine, and 5.5mM glucose) on ice. Still-beating hearts were then cannulated and perfused for 5 min with PB before digestion with type 2 collagenase (Worthington Biochemical Corp., Lakewood, NJ) in PB. Following approximately 35 min digestion, ventricles were cut away from atria, teased into smaller pieces, and transferred to PB supplemented with 12.5µM $CaCl_2$ and 1% bovine serum albumin. Following 10 min of gravity sedimentation at room temperature, CM were reintroduced to calcium with step-wise additions of 0.25mM, 0.25mM, 0.5mM, 0.5mM, and 0.3mM $CaCl_2$ to ensure calcium-tolerant CM for plating. Viable CM were counted with Trypan Blue and hemocytometer before seeding to 18µg/mL laminin-coated 35mm glass-bottom FluoroDishes (World Precision Instruments) at 51,000 CM/dish or to Seahorse XF24 V7 PS cell culture microplates (3WK at 17,000 CM/well; 10WK and 6MO at 10,000 CM/well; 12MO at 6,000 CM/well) for Extracellular Flux Analyses or 3,000 12MO CM/well for Permeabilized Extracellular Flux Analyses in MEM (Gibco Cat. #11575032, Grand Island, NY) containing 2mM L-glutamine and 5.6mM D-glucose. CM were allowed to attach for at least 1 hr before experimentation. As authors observed functional and morphologic differences in CM (particularly from 12MO offspring) with the amount of time in culture, consistent experimental timing was prioritized.

Echocardiography

Structural and functional cardiac physiology was followed over time using serial echocardiography at P1, 3WK, 10WK, 6MO, and 12MO as previously detailed (Baack et al., 2016; Mdaki et al., 2016a). In short, echocardiography was done using the Vevo 2100 Imaging System (FUJIFILM VisualSonics Inc., Toronto, Canada). While under light (1-3%) isoflurane/oxygen anesthesia, hair was removed from the ventral chest, and offspring were secured on a prewarmed (37C) imaging stage with embedded electrocardiogram leads. Temperature and EKG were monitored continuously to assure physiologic stability. Parasternal long axis (PLAX), parasternal

short axis (PSAX), and the apical four chamber views were acquired in B mode (brightness), M mode (motion), and pulsed-wave (PW) Doppler mode using MS700 (P1), MS400 (3WK), or MS250 (10WK-12MO) MicroScan high-frequency transducers according to animal size (FUJIFILM VisualSonics Inc.). All echocardiograms were acquired by one trained individual, and image analysis was done by a separate technician using the Vevo LAB analysis software (FUJIFILM VisualSonics Inc.). Reported ventricular measurements are from left ventricular trace in PLAX, systolic function (ejection fraction and fractional shortening) is from M mode in PSAX, and diastolic function (E:A ratio) is from PW Doppler apical images. Right ventricular function is reported as the ratio of pulmonary artery acceleration time (PAAT) to right ventricular ejection time (RVET) as calculated from PW Doppler modified PLAX images of the right ventricular outflow tract (RVOT).

Hepatic Lipid Analyses

Whole livers were weighed and snap frozen in liquid nitrogen immediately upon collection and stored at -80C for future processing and analyses. For hepatic TG analysis, liver tissue (100mg) was homogenized in 1mL of an aqueous 5% NP-40 solution, heated at 90C for 10 min, and spun at top speed in a microcentrifuge for 2 min. TG concentrations in liver extracts were quantified with a commercial kit (Zenbio, STG-1-NC) according to manufacturer's instructions. Hepatic cholesterol was extracted and analyzed by gas chromatography as previously described (Rideout et al., 2015).

Serum Analyses

Blood was collected from dams and offspring via venipuncture or intracardiac puncture under anesthesia or immediately following humane euthanasia. Whole blood and serum fractions were stored at -80C for analysis. To validate fetal hyperinsulinemia, a subset of P1 offspring (n=40-68 pups/group) was delivered by cesarean section with immediate jugular venous sampling prior to cutting the umbilical cord as previously described (Louwagie et al., 2018). Milliplex MAP Magnetic Bead Panels (MilliporeSigma, Burlington, MA) with Luminex 200 Analyzer (Luminex Corp, Austin, TX) were used to measure serum concentrations of insulin, C-peptide, and leptin (Cat. #RMHMAG-84K) as well as adiponectin, E-selectin, and ICAM-1 (Cat. #RV2MAG-26K). Serum HbA1c levels were measured with Rat Hemoglobin A1C Assay Kit (Cat. #80300, Crystal Chem, Elk Grove Village, IL), brain natriuretic peptide with Rat BNP 45 ELISA Kit (Cat. #ab108816, Abcam, Cambridge, MA), serum TG with Pointe Scientific colorimetric assay and TG standards (Cat. #23-666-410 and #23-666-422, ThermoFisher Scientific, Waltham, MA), and NEFA levels with Wako HR Series NEFA-HR Colorimetric Kit (Wako Diagnostics, Richmond, VA). Serum total and HDL cholesterol was measured using EnzyChrom AF HDL and LDL/VLDL Assay Kit (Cat. # E2HL-100, Universal Biologics, Cambridge, UK); non-HDL cholesterol (representing VLDL, IDL, LDL, chylomicron remnants and lipoprotein) was calculated by subtracting HDL from total cholesterol. Serum renin concentrations were measured with SensoLyte 520 Rat Renin Assay Kit (Cat. #AS-72140, Anaspec, Fremont, CA). All assays were run per manufacturer's instructions and read on Cytation3 plate reader (BioTek, Winooski, VT) unless otherwise noted.

Extracellular Flux Analyses

CM bioenergetics were assessed using a mitochondrial stress test (MST), glycolytic stress test (GST), and fatty acid oxidation test (FAOT) on Seahorse XF24 extracellular flux analyzer at all five time points. Methods have been previously described in detail (Mdaki et al., 2016a). Specifically, before beginning each assay CM were washed twice in assay media and incubated for 1hr in absence of CO_2. Oxygen consumption rates (OCR) and extracellular acidification rates (ECAR) were measured at baseline and following injections to determine respiratory, glycolytic, and FAO capacities. All media were heated to 37C with pH adjusted to 7.40. Assays used the following injection strategies (listed concentrations are final) and media types:

***MST*:** 2μM Oligomycin, FCCP (0.3μM for P1, 0.6μM for 3WK-6MO, 0.9μM for 12MO), and then 2μM rotenone plus 4μM Antimycin A; XF assay medium supplemented with 10mM glucose and 1mM pyruvate.

***FAOT (P1-6MO)*:** 0.15mM Palmitate-BSA conjugate followed by two injections of 40μM etomoxir; KHB medium (111mM NaCl, 4.7mM KCl, 1.25mM $CaCl_2$, 2mM $MgSO_4$, 1.2mM NaH_2PO_4) supplemented with 0.5mM carnitine, 2.5mM glucose, and 5mM HEPES.

***FAOT (12MO)*:** 4μM Oligomycin, 0.9μM FCCP, and then 2μM rotenone plus 4μM Antimycin A. Run in four different conditions (with 0.15mM Palmitate-BSA conjugate or BSA control +/- 30 min 40μM etomoxir pretreatment) to determine both basal and palmitate-stimulated oxidation as well as reserve capacities for endogenous and exogenous FA oxidation (Rogers et al., 2014); KHB medium supplemented with 0.5mM carnitine, 2.5mM glucose, and 5mM HEPES.

***GST*:** 10mM Glucose, 2μM Oligomycin (P1-6MO) or 2μM rotenone plus 4μM Antimycin A (12MO), and then 100mM 2-deoxyglucose (P1-6MO) or 100μM Monensin (12MO) to additionally ascertain maximal and glycolytic reserve capacities (Mookerjee et al., 2016); XF base medium. Proton production rate (PPR) was calculated as described by Mookerjee et al (Mookerjee et al., 2015).

Oil Red O Staining and Quantification

Following euthanasia, right ventricle section from 12MO hearts were frozen in optimal cutting temperature (O.C.T.) tissue preservative (Sakura Finetek) and stored at -80C. Batched hearts were sectioned (10μm), fixed with 40% formaldehyde, stained for 10 min with Oil Red O (Sigma-Aldrich) suspended in 98% isopropanol, stained with hematoxylin (background), and blued in ammonia water before mounting. Five to six images per heart were systematically captured using an Aperio Versa 8 microscope (Leica

Biosystems) at 40x magnification. Oil Red O was systematically quantified using ImageJ (NIH) with Color Threshold settings of Hue at 119-210 (no pass), Saturation at 4-255, and Brightness at 66-195.

Mitochondrial DNA Copy Number

Snap-frozen hearts from all five time points were used to isolate total DNA using a Qiagen DNeasy Blood and Tissue Kit according to manufacturer's instructions. Relative mtDNA copy number was then determined using real-time PCR as previously described (Mdaki et al., 2016a). All reactions were performed in triplicate using ABsolute Blue QPCR Mix (ThermoFisher Scientific) and a Stratagene Mx3000P thermocycler (Agilent Technologies). Primers were designed for cytochrome-c oxidase I (Mt-co1; ThermoFisher). Methods were previously validated using a second primer for mitochondrial control region (D-loop; Integrated DNA Technologies) as previously described (Mdaki et al., 2016a). Gene-specific standard curves were generated with MxPro software (Agilent Technologies) and used to calculate relative mtDNA copy number.

Permeabilized Cell Analyses

To determine mitochondrial electron transport chain complex function, CM from P1 and 12MO CM mitochondria were evaluated using extracellular flux analyses after permeabilization via 1nM Seahorse XF Plasma Membrane Permeabilizer as described by Salabei, et al (Salabei et al., 2014). CM isolation was as described for MST, GST, and FAOT above and methods were technically similar and illustrated in Figure 5A. Key exceptions include: CM were only washed once and assay was started immediately following wash. MAS assay medium (220mM mannitol, 70mM sucrose, 10mM KH_2PO_4, 5mM $MgCl_2$, 2mM HEPES, 1mM EGTA, 0.6% FA-free BSA) was heated to 37C with pH adjusted to 7.20 before washing. Seeding density, fuel and drug doses were validated at each time point according to the manufacturer's recommendations. Injection strategies were as follows (listed concentrations are final):

***P1 CM*: (**10mM methyl pyruvate plus 2mM dichloroacetate plus 1mM malate) or (4mM glutamine plus 1mM malate) or (40µM palmitoyl-L-carnitine plus 1mM malate) or (10mM succinate) or (0.5mM duroquinol) or (0.1mM N,N,N′,N′-tetramethyl-p-phenylenediamine (TMPD) plus 5mM ascorbate) with 4mM ADP and 1nM XF PMP permeabilizer, next 2µM Oligomycin, and then lastly (2µM rotenone plus 4µM Antimycin A for complex I and II wells) or (40mM sodium azide for complex III and IV wells).

***12MO CM*:** Modification to P1 CM methods include the following differences: 50µM palmitoyl-L-carnitine, 0.5mM TMPD, and 2mM ascorbate. ADP and permeabilizer were added to final wash step, prior to the run (rather than with first injection as in P1 CM). This was done to ensure more time for complete permeabilization. Lastly, while evaluating complex III oxidation of duroquinol, a second injection of 40mM sodium azide was done to ensure complete inhibition prior to TMPD/ascorbate.

FCCP Challenge

***Staining and Imaging*:** 12MO CM were transferred from MEM to 2mL confocal solution (Seahorse XF Assay Medium [Agilent] + 10mM D-(+)-glucose [Sigma] + 1.0mM sodium pyruvate [Sigma]) containing 1.0µM MitoTracker Green FM (Invitrogen, Waltram, MA) + 2.0µM Hoechst 33342 (AnaSpec, Fremont, CA) + 15nM Tetramethylrhodamine Ethyl Ester Perchlorate (TMRE) (Invitrogen) or 1.0µM LysoTracker Red DND-99 (Invitrogen) and incubated for 20 min at 37C with humidified, 2% CO_2. CM were washed twice with 1xPBS and given fresh confocal medium for imaging. All staining procedures were conducted in minimal lighting with dark tubes and light-protected culture dishes to minimize photobleaching.

Images were captured using a Nikon A1 TIRF Ti-Eclipse inverted confocal microscope (Nikon Instruments Inc., Melville, NY) equipped with a live cell chamber (37C with humidified 5% CO_2), Nikon Perfect Focus System, injection apparatus, and NIS-Elements AR image acquisition software (version 5.02; Nikon). Individual CM were selected for imaging in a standard manner by a single technician based on morphology and stain quality at the start of imaging. Baseline images were obtained and video was captured using Perfect Focus System throughout. Two minutes after beginning video acquisition, FCCP was cautiously injected (final concentration = 0.6µM) as not to interrupt the cells. Imaging was maintained through cell death. Importantly, each video capture was performed using standardized parameters at x60 magnification and 1024x1024 pixels with 1.1µs pixel dwell (6.27 seconds/frame). Representative video-images are shown in Figures 6 and 7. Representative videos are online as Supplementary Videos S1 (Mitophagy) and S2 (Cell Death).

***Image Analyses*:** NIS-Elements' Measure tool was used to estimate baseline cell morphology and time to cell death by retraction, defined as the first post-FCCP frame in which cell length became 50% of baseline. Videos were exported as sequential Tagged Image Format (TIF) files into High-Content Screening (HCS) Navigator software (version 6.6.0; PerkinElmer, Waltham, MA) using the Image Import and Conversion Tool. Following conversion, videos were analyzed using HCS Colocalization.V4 protocol for TMRE intensity, colocalization, and time to cell death by pyknosis, defined as the first post-FCCP frame in which nuclear area became 90% of baseline. ROI recognition settings were adjusted to place a mask around the CM of interest from each frame. This step was necessary to remove artifacts and focus on individual CM. ROI settings were standardized between all samples. Data were exported using the HCS Data/Image Export Tool.

Protein Isolation and Western Blotting

Left ventricle sections were homogenized and sonicated in RIPA (150mM NaCl, 50mM Tris (pH=7.5), 1% Triton X, 0.5% deoxycholate, 0.1% sodium dodecyl sulfate) supplemented with cOmplete Protease Inhibitor Cocktail (Roche, Indianapolis IN) and phosphatase inhibitor cocktail (Sigma-Aldrich, St. Louis, MO). Proteins were quantified using DC Protein Assay (Bio-Rad, Hercules,

CA) and Cytation3 plate reader (BioTek, Winooski, VT). Western solutions were prepared with Laemmli and beta-mercaptoethanol, heated at 95C for 5 min, and run through 4-15% Criterion TGX gels (Bio-Rad) alongside EZ-Run Prestained Rec Protein Ladder and MagicMark XP Western Protein Standard (ThermoFisher, Waltham, MA). 20µg protein was loaded per lane. Transfer to PVDF membranes was performed using Trans-Blot Turbo Transfer System (Bio-Rad). Membranes were blocked for 10 min in 10% Clear Milk Blocking Buffer (ThermoFisher) before overnight incubation with primary antibody at 4C. Following TBS-T washes, membranes were again blocked and incubated 1 hr in secondary antibody. Membranes were washed four times before imaging with Luminata Forte HRP Chemiluminescence Substrate (ThermoFisher) and ChemiDoc MP Imaging System (Bio-Rad) with Image Lab Touch Software (version 2.2.0.08; Bio-Rad). Densitometry was performed using VisionWorks LS Analysis Software (version 8.1.2, UVP, Upland, CA). Before analysis, image brightness and contrast was uniformly adjusted using Adobe Photoshop (version 13.0; Adobe Inc., San Jose, CA) to capture bands in their entirety. Beta-actin served as reference protein (Figure S6E). All antibodies are shown in the below table.

Antibody	Source	Identifier
Anti-DRP1 (H-300), diluted 1:350	Santa Cruz Biotechnology	Cat#SC-32898
Anti-MFF, diluted 1:1000	Cell Signaling Technology	Cat#84580; RRID:AB_2728769
Anti-MTFP1, diluted 1:1000	Antibodies-online	Cat#ABIN3047683
Anti-MFN1, diluted 1:200	Santa Cruz Biotechnology	Cat#SC-50330; RRID:AB_2250540
Anti-MFN2, diluted 1:1000	Sigma-Aldrich	Cat#M6319; RRID:AB_477221
Anti-OPA1, diluted 1:1000	Cell Signaling Technology	Cat#80471; RRID:AB_2734117
Anti-DAP3, diluted 1:1000	BD Biosciences	Cat#610662; RRID:AB_397989
Anti-VDAC1/Porin, diluted 1:1000	Abcam	Cat#Ab14734; RRID:AB_443084
Anti-CYPD, diluted 1:1000	Abcam	Cat#Ab110324; RRID:AB_10864110
Anti-NDUFA2, diluted 1:500	LifeSpan Biosciences	Cat#LS-C409672
Anti-SDHA, diluted 1:5000	Abcam	Cat#ab14715; RRID:AB_301433
Anti-UQCRH, diluted 1:5000	Abcam	Cat#ab134949; RRID:AB_2800504
Anti-COX5B, diluted 1:10,000	Abcam	Cat#ab180136
Anti-ADRP, diluted 1:1000	Abcam	Cat#ab108323; RRID:AB_10863476
Anti-β-Actin (HRP-conj.), diluted 1:1000	Cell Signaling Technology	Cat#5125S; RRID:AB_1903890
Goat anti-rabbit IgG-HRP, diluted 1:5000	SouthernBiotech	Cat#4030-05; RRID:AB_2687483
Goat anti-mouse IgG(H+L) human ads-HRP, diluted 1:5000	SouthernBiotech	Cat#1031-05; RRID:AB_2794307

Experimental Optimization

Non-experimental rats were used to optimize cell seeding densities, reagent concentrations, and staining/imaging parameters. To do this, CM were isolated from each time point as described above and seeded onto Seahorse XF24 V7 PS cell culture microplates or FluoroDishes. MST (see above) was used to determine the FCCP concentrations that elicit maximal respiratory capacities. MST methods have previously been described in detail (Mdaki et al., 2016a; Mdaki et al., 2016b), but optimization steps for this study compared 0.1-1.2µM FCCP. Although 0.9µM FCCP elicited the maximal respiratory capacity in plated 12MO CM, the concentration causing the second-highest response (0.6µM) was chosen to prevent over-stressing and immediate cell death under harsher confocal imaging conditions.

Statistical Analyses

All statistical analyses were conducted using Prism 7.05 (GraphPad Software) and are represented as mean ± standard error of the mean. Statistical parameters including replicate numbers (n) are shown in tables and figure legends. Diabetes, diet, and interaction effects were evaluated by two-way ANOVA. When a significant interaction was present, data were analyzed by one-way ANOVA with Dunnett post-test to compare each treatment group (diabetes, HF diet, or combination) to controls. Sex-specific comparisons were interrogated by two-tailed, unpaired t-test. For mitolysosome formation, Pearson correlation coefficient values were calculated from baseline to time of cell death for each video frame and interrogated by linear regression analysis. Baseline levels of mitolysosomes and rate of mitolysosome formation were analyzed by ANOVA as described above. Rate of mitochondrial biogenesis, defined as the rise in mitochondrial copy number over time (P1 to 12MO), was also interrogated using similar linear regression analyses. To compare age-related differences, one-way ANOVA was used to compare time points within exposure groups and linear regression analysis and two-way ANOVA were used to compare rates of change between groups from P1 to 12MO. Statistical significance was set to $P<0.05$ for all cases.

SUPPLEMENTAL REFERENCES

Mookerjee, S.A., Goncalves, R.L.S., Gerencser, A.A., Nicholls, D.G., and Brand, M.D. (2015). The contributions of respiration and glycolysis to extracellular acid production. Biochimica et biophysica acta *1847*, 171-181.
Rideout, T.C., Movsesian, C., Tsai, Y.-T., Iqbal, A., Raslawsky, A., and Patel, M.S. (2015). Maternal phytosterol supplementation during pregnancy and lactation modulates lipid and lipoprotein response in offspring of apoE-deficient mice. J Nutr *145*, 1728-1734.
Salabei, J.K., Gibb, A.A., and Hill, B.G. (2014). Comprehensive measurement of respiratory activity in permeabilized cells using extracellular flux analysis. Nature protocols *9*, 421-438.